Check for updates

AGU ADVANCING EARTH AND SPACE SCIENCES

JGR Planets

RESEARCH ARTICLE

10.1029/2025JE008943

Key Points:

- SuperCam Raman acquisition and processing procedures have been optimized, demonstrating remarkable performance for a standoff configuration
- SuperCam Raman can aptly differentiate chemical compositions, hydration states, and quantify cation content in minerals and salts on Mars
- Raman spectroscopy has been essential for understanding Jezero's geology, and will play a key role in future planetary exploration missions

Supporting Information:

Supporting Information may be found in the online version of this article.

Correspondence to:

G. Lopez-Reyes,
guillermo.lopez@uva.es

Citation:

Lopez-Reyes, G., Manrique, J. A., Clavé, E., Ollila, A., Beyssac, O., Pilleri, P., et al. (2025). SuperCam Raman activities at Jezero Crater, Mars: Observational strategies, data processing, and mineral detections during the first 1,000 sols. *Journal of Geophysical Research: Planets*, *130*, e2025JE008943. https://doi.org/10.1029/2025JE008943

Received 13 FEB 2025
Accepted 28 OCT 2025

Author Contributions:

Writing – original draft: J. A. Manrique, E. Clavé
Writing – review & editing: J. A. Manrique, E. Clavé

© 2025. The Author(s).
This is an open access article under the terms of the Creative Commons Attribution-NonCommercial-NoDerivs License, which permits use and distribution in any medium, provided the original work is properly cited, the use is non-commercial and no modifications or adaptations are made.

SuperCam Raman Activities at Jezero Crater, Mars: Observational Strategies, Data Processing, and Mineral Detections During the First 1000 Sols

G. Lopez-Reyes[1], J. A. Manrique[1], E. Clavé[2], A. Ollila[3], O. Beyssac[4], P. Pilleri[5], S. Bernard[4], E. Dehouck[6], M. Veneranda[1], S. K. Sharma[7], M. Nachon[8], J. Aramendia[9], O. Forni[5], F. Rull[1], T. Acosta-Maeda[7], A. Brown[10], S. M. Angel[11], K. Castro[9], E. Cloutis[12], L. Coloma[9], J. Comellas[7], D. Delapp[3], R. Jakubek[13], S. Julve-Gonzalez[1], E. Kelly[7], J. M. Madariaga[9], G. Montagnac[6], I. Poblacion[9], S. Schröder[2], S. A. Connell[14], I. Reyes-Rodriguez[1], Z. U. Wolf[3], S. Maurice[5], O. Gasnault[5], S. Clegg[3], A. Cousin[5], R. C. Wiens[14], and the SuperCam Raman Working Group and the SuperCam Team[15]

[1]ERICA Research Group and LaDIS. Universidad de Valladolid (Spain), Valladolid, Spain, [2]Deutsches Zentrum für Luft- und Raumfahrt e.V. (DLR), Institute of Space Research, Berlin, Germany, [3]Los Alamos National Laboratory (LANL), Los Alamos, NM, USA, [4]IMPMC, Institut de Minéralogie, de Physique des Matériaux et de Cosmochimie, CNRS, Sorbonne Université, MNHN, Paris, France, [5]Institut de Recherche en Astrophysique et Planétologie (IRAP), Université de Toulouse 3 Paul Sabatier, CNRS, CNES, Toulouse, France, [6]Université Claude Bernard Lyon 1, ENS de Lyon, CNRS, UJM, LGL-TPE, UMR 5276, Villeurbanne, France, [7]University of Hawai'i at Mānoa, Honolulu, HI, USA, [8]Texas A&M University, College Station, TX, USA, [9]University of the Basque Country (UPV/EHU), Bilbao, Spain, [10]Plancius Research, Severna Park, MD, USA, [11]Department of Chemistry and Biochemistry, University of South Carolina, Columbia, SC, USA, [12]University of Winnipeg, Winnipeg, MB, Canada, [13]Jacobs, NASA Johnson Space Center, Houston, TX, USA, [14]Purdue University, West Lafayette, IN, USA, [15]See Appendix A

Abstract The Mars 2020 Perseverance rover introduced Raman spectroscopy to in situ planetary exploration for the first time when it landed in Jezero crater on Mars in February 2021. The SuperCam instrument onboard Perseverance is a multi-analytical tool capable of acquiring time-resolved Raman data from Martian targets at standoff distances of a few meters. This is a particularly challenging task due to the operational constraints, the harsh conditions on the Martian surface, and especially the very fine-grained nature of the Martian soil. To address these challenges, the SuperCam Raman team has invested significant effort into optimizing both the acquisition and post-processing of Raman data collected on Mars, as detailed in this work. Additionally, this paper reviews and discusses the detections made by SuperCam Raman during the first 1,000 sols (almost 3 Earth years) of the Mars 2020 mission. During this period, SuperCam Raman data provided key insights into the mineralogy of Jezero throughout the Crater, Delta, and Margin Campaigns. Key detections include olivine, carbonates, perchlorates, and sulfates (such as anhydrite), identified in both abraded patches and natural surfaces. The high specificity of Raman spectroscopy enables the unequivocal identification of these minerals, allowing for rapid and direct interpretation of Jezero's mineralogy, especially when combined with other techniques from SuperCam or others on the rover. Furthermore, this paper compiles the spectra acquired from the SuperCam Calibration Target samples on Mars, including studies on the degradation of the Ertalyte (PET), an organic polymer sample and analyses of diamond, apatite, and other reference materials.

Plain Language Summary The SuperCam instrument onboard Mars 2020 Perseverance rover performs Raman spectroscopy on Martian targets. The SuperCam team has made significant efforts to optimize Raman data acquisition and processing to maximize its scientific return. This paper summarizes these efforts, while also presenting all the Raman data acquired during the first 1,000 sols of the Perseverance mission in Jezero crater—including the first Raman spectrum ever obtained from another planetary surface. Additionally, we discuss how these analyses have been critical for interpreting the geologic history of Jezero, and show that Raman is a powerful technique for planetary exploration missions.

1. Introduction

The Perseverance rover, which landed in Jezero Crater (Mars) in February 2021, carries the SuperCam instrument suite (Manrique et al., 2020; Maurice et al., 2021; Wiens et al., 2021), that combines several analytical techniques: laser-induced breakdown spectroscopy (LIBS), time-resolved Raman spectroscopy, time-resolved luminescence

spectroscopy (TRLS), visible and near-infrared reflectance spectroscopy (VISIR), as well as a Remote Micro-Imager (RMI), and a microphone that records acoustic data to analyze the physical properties of rocks and the Martian atmosphere (Maurice et al., 2021, 2022). Raman spectroscopy is a powerful technique for the analysis of materials by exciting them with a monochromatic source of light, typically a laser. Indeed, as each molecule and mineral exhibit a unique and characteristic pattern of inelastically scattered light, Raman spectroscopy can provide information about the molecular structure, composition of both organic and inorganic molecules found on Mars (e.g., Böttger et al., 2012).

Because of the constraints imposed to space hardware, conducting Raman spectroscopy on a different planet is challenging, especially with a standoff Raman instrument (Angel et al., 2012; Sharma et al., 2003; Wiens et al., 2017). Nevertheless, the Raman data provided by SuperCam has proven to be effective for the identification of mineral species on the surface of Mars. During the first 1,000 sols of operations on Mars, SuperCam has analyzed ~500 points on 60 geological targets, plus a few tens of analytical activities on the SuperCam calibration targets that are attached to the rover and can be measured regularly. Considering the relatively high consumption of laser shots compared to LIBS (100–400 per point for Raman vs. typically 30 for LIBS), the SuperCam team has prioritized high-interest targets (such as rocks abraded by the rover) within a relatively short range (<~5 m) for Raman analyses. Nonetheless, the set of Raman data acquired so far by SuperCam has provided key insights into Martian mineralogy, confirming the significant potential and utility of this technique for planetary in situ exploration.

Considering the inherent challenges associated with Martian conditions and the operational constraints of the instrument, a robust data acquisition procedure is imperative to maximize the scientific return of the acquired data. One challenge is that the standoff configuration of the instrument limits the signal-to-noise ratio (SNR) compared to typical laboratory instruments. This underscores the necessity for meticulous optimization of the Raman spectra acquisition process. To this end, the SuperCam Team designed different characterization activities aimed at maximizing the collection of Raman signals, including optimizing the number of shots, studying the optimal on-chip accumulations or "coadds" (number of laser pulses and simultaneous intensifier activations in one detector readout), laser power and/or frequency, or even distance to samples. Throughout these activities, a comprehensive understanding of the instrument's behavior was obtained, characterizing potential artifacts or the influence of environmental factors on spectral quality.

On the other hand, a robust data post-processing framework is also key. Taking into account the unique features exhibited in SuperCam Raman spectra (the presence of spikes -intense spurious peaks such as cosmic rays- and a "fiber bump" -a spectral artifact attributed to Raman excitation within the optical harness of the instrument's collection system by reflected laser light-), demand the use of post-processing techniques for the effective removal of noise, spikes, and artifacts. The effort carried out by the SuperCam Raman Working Group and the SuperCam Team in this regard is described as part of this work.

The SuperCam instrument suite has significantly contributed to the interpretation of the Jezero crater geology by systematically combining all its analytical techniques. This integrated strategy has proven highly effective for robust mineralogical analysis. This work compiles the Raman analyses performed by SuperCam over the first 1,000 sols of the mission both on Mars rock targets and on the SuperCam Calibration Targets (Manrique et al., 2020), acquired from February 2021 through December 2023.

2. Mission Context

2.1. Jezero Crater, Mars

Jezero Crater, located in the Nili Planum region of Mars, was selected as the landing site for NASA's Mars 2020 mission due to its unique geological and astrobiological significance (Farley et al., 2020). Jezero is a ~45-km-diameter crater that once housed an open-system lake more than 3.5 billion years ago, during the Noachian period. This period is marked by notable aqueous activity, evidenced by the presence of valley networks, channels, and diverse hydrated mineral assemblages throughout the region (Ehlmann, Mustard, Murchie, et al., 2008, Ehlmann, Mustard, Fassett, et al., 2008; Goudge et al., 2015). The crater features a well-preserved delta and carbonate-bearing rocks, making it a prime candidate for studying ancient habitable environments and the preservation of biosignatures (Farley et al., 2020). The surrounding Nili Planum highlands, into which Jezero impacts, host

21699100, 2025, 11, Downloaded from https://agupubs.onlinelibrary.wiley.com/doi/10.1029/2025JE008943, Wiley Online Library on [18/11/2025]. See the Terms and Conditions (https://onlinelibrary.wiley.com/terms-and-conditions) on Wiley Online Library for rules of use; OA articles are governed by the applicable Creative Commons License

some of the best-preserved Noachian landscapes, further enriching the scientific value of the site with a diverse array of altered rocks and sediments (Farley et al., 2020).

Jezero Crater's geography is marked by several distinct regions: crater floor, delta and carbonate-rich rocks in the margin unit. Two main units had been identified from orbit in the crater floor: the light-toned floor and the mafic floor (Goudge et al., 2015). The mafic floor appeared olivine-rich and possibly related to the regional olivine-bearing unit covering 18,000 km^2 in the Nili Fossae region (Goudge et al., 2015; Hoefen et al., 2003; Mandon et al., 2021) it was interpreted as igneous in origin. The origin of the light-toned floor was less clear, either sedimentary or igneous. The Western delta in the Neretva Vallis was identified as a key target for astrobiological exploration due to its potential to preserve ancient biosignatures (Farley et al., 2020). The interior of the crater rim shows particularly strong carbonate signatures as observed from orbit, hypothesized (among others) to have formed in the shore zone of a lake (e.g., Horgan et al., 2020).

2.2. The Mars 2020 Mission Scientific Campaigns

The Perseverance rover has successfully completed over 1,000 sols on Mars, addressing several scientific campaigns. During the initial months of the mission, spanning from sols 100 to 414, Perseverance conducted the Crater Floor campaign (Simon et al., 2023; Sun et al., 2023). This campaign focused on analyzing the Máaz and Séítah formations within the Jezero crater floor, corresponding to the light-toned and mafic floor units identified from orbit, respectively. This campaign involved traversing more than 5 km and the examination of 7 abrasion patches and many natural surface targets. Perseverance observations have revealed the crater floor to be predominantly volcanic and intrusive, featuring a basaltic lithology enriched with plagioclase, and pyroxene on Máaz, along with an olivine cumulate in the stratigraphically lower unit, Séítah (Farley et al., 2020; Wiens et al., 2022). The Máaz formation consists of different lava flows and/or possibly pyroclastic flows with complex textures, including vesicular and non-vesicular rocks with different grain sizes (Udry et al., 2022). The Séítah formation is the stratigraphically lowest geological unit that was exposed at the bottom of the Jezero crater and could thus be explored. It consists of magmatic, olivine-rich rock that was formed by fractional crystallization and slow cooling of magma, subsequently exhumed by erosion (Beyssac et al., 2023; Liu et al., 2022). Significantly, both formations display evidence of multiple episodes of aqueous alteration, highlighted by the presence of secondary minerals such as carbonates, Fe/Mg phyllosilicates, amorphous silicates, sulfates, perchlorates, and Fe-silicates (Clavé, Benzerara, et al., 2023; Corpolongo et al., 2022; Lopez-Reyes et al., 2023; Mandon et al., 2023; Meslin et al., 2022; Nachon, Lopez-Reyes, et al., 2024; Sun et al., 2023; Tice et al., 2022).

The study of the Jezero delta, one of the primary objectives of the Mars 2020 mission, extended over 500 sols from mission sols 415 to 909, including two distinct campaigns-the fan front and the upper fan (delta top) campaigns, with the overall objective of understanding the nature of the Western fan. The observations unveiled a remarkable compositional diversity including serpentine, clays, sulfates, and carbonates. These findings suggest a complex aqueous history with diverse past geochemical environments in the Jezero delta region (Bosak et al., 2024; Dehouck, Clavé, et al., 2024, Dehouck, Forni, et al., 2024; Nachon, Lopez-Reyes, et al., 2024, Nachon, Clegg, et al., 2024; Siebach et al., 2023).

The Margin Campaign (sols 910 onwards) focused on investigating the Margin Unit, a pre-delta formation (Horgan et al., 2024) showcasing extensive carbonate-bearing mineralogy as observed from orbit (Edwards & Ehlmann, 2015; Goudge et al., 2015; Horgan et al., 2020; Tarnas et al., 2021; Zastrow, 2021). Despite extensive in situ investigation with Perseverance, multiple hypotheses are still being considered regarding the origin of these rocks, including sedimentary, pyroclastic, and volcanic igneous, with extensive carbonation of olivine, among other alteration processes (Clavé, Beck, Beyssac, et al., 2024; Horgan et al., 2024).

2.3. The SuperCam Instrument

The SuperCam instrument on NASA's Mars 2020 Perseverance rover is a versatile remote-sensing tool designed to study the geology of Mars, which has been described in detail elsewhere (Beyssac et al., 2023; Manrique et al., 2020; Maurice et al., 2021; Wiens et al., 2021). As explained, it combines several analytical techniques on a standoff configuration, allowing analysis of minerals and rocks at distances of several meters. SuperCam provides high-resolution contextual images as the RMI captures detailed images from distances up to kilometers. VISIR analysis facilitates mineral identification and atmospheric studies by analyzing reflected light in the visible (0.40–0.85 μm) and near-infrared (1.3–2.6 μm) ranges.

21699100, 2025, 11, Downloaded from https://agupubs.onlinelibrary.wiley.com/doi/10.1029/2025JE008943, Wiley Online Library on [18/11/2025]. See the Terms and Conditions (https://onlinelibrary.wiley.com/terms-and-conditions) on Wiley Online Library for rules of use; OA articles are governed by the applicable Creative Commons License

Elemental analysis by LIBS is performed by generating plasma on the samples with a 1,064 nm pulsed laser, with a frequency of 10 Hz, and a 4 ns pulse width (Maurice et al., 2021). The advanced multivariate and machine learning analysis of SuperCam LIBS data allows obtaining quantitative information of the elemental composition of samples (Anderson et al., 2021), facilitating mineralogical interpretation of the data.

When operating in Raman mode, SuperCam uses a 532 nm excitation wavelength by frequency doubling the 1,064 nm pulsed laser source (Maurice et al., 2021), acquiring up to 400 shots per analyzed point. By performing time-resolved spectroscopy, SuperCam Raman rejects the long recombination time background luminescence using a 100 ns gated detector, only capturing signals within 100 nanoseconds after firing of the laser pulse. The Raman light is collected by a transmission spectrometer featuring an intensifier, which provides a spectral resolution better than 12 cm^{-1} in the Raman spectral range between around 140 and 4,000 cm^{-1} (Wiens et al., 2021).

The TRLS analysis by SuperCam is achieved by using longer delays and/or time gates during which the signal is acquired post laser pulse, enabling the acquisition of luminescence emission signals in the range of 535–855 nm (Wiens et al., 2021).

3. SuperCam Raman Data Acquisition and Processing

The SuperCam instrument on Mars produces raw data, which is pre-processed onboard the Perseverance rover to produce a packet of uncalibrated data in a format known as eXtracted Data Record (XDR). To convert this raw data into a refined and scientifically usable format, an automated data pipeline is employed upon reception of the data on Earth, resulting in Experimental Data Record (EDR) files. This pipeline further processes data performing a series of automated operations on the spectra, correcting instrumental biases, calibrating the data, reducing noise, and handling artifacts. The outcome of the pipeline is the Clean Data Record (CDR), which serves as the basic data set for subsequent scientific analyses. However, the scientific team retains access to the XDR and EDR files, allowing customized processing of the data when needed.

The success of the SuperCam Raman instrument in acquiring meaningful data on Mars is noteworthy given the challenges associated with the inherently weak Raman effect itself, combined with the additional limitations of a standoff configuration working at relatively long distances up to ~7 m with a limited number of shots (max 2,000 laser shots per target to prevent overheating the instrument). As a result, some of the acquired Raman spectra from SuperCam presents a low SNR. This was expected and had experimentally been shown in different earth-based developments (Angel et al., 2012; Beyssac, 2020; Manrique et al., 2024; Rull et al., 2011; Sharma et al., 2003, 2007, 2009; Wiens et al., 2005, 2021). In this context, proper data processing is critical to maximize scientific return from the instrument data.

Given the critical significance of the data processing methodologies applied to SuperCam Raman spectra, the following sections thoroughly describe these processes. First, the optimization of the acquisition process is addressed, followed by a description of data processing techniques employed for the interpretation of SuperCam Raman data. Many of the post-processing algorithms described in this work are inherited from the ChemCam LIBS instrument on the Curiosity rover (Maurice et al., 2012; Wiens et al., 2013), while others are specific and have been developed for SuperCam Raman spectroscopy, such as the despiking of spectra or the correction of instrumental artifacts. Most of these processes have been implemented into the SuperCam python-based data processing pipeline, while the development work has been done profiting from the already-existing routines or libraries in the pipeline, or by external software such as MATLAB, SpectPro (Veneranda et al., 2021) or other programming languages or spectral processing software.

It is important to note that the SuperCam Raman spectra exhibit a notable artifact—a substantial bump (hereafter referred to as the "fiber bump") in the 200–500 cm^{-1} region, accompanied by weaker features at approximately 600 cm^{-1}, 800 cm^{-1}, and 1,050 cm^{-1} (see Figure S1 in Supporting Information S1). This artifact is attributed to the backscattered laser light, which excites the molecular vibrations of SiO_2 (Chligui et al., 2010) within the optical 5.8 m long x 300 μm diameter optical fiber between the telescope and the spectrometers (Wiens et al., 2021). This feature was recognized early in the design phase and an optical filter was added at the back of the telescope to remove most (94%) of the back-reflected 532 nm light (Maurice et al., 2021). It was not possible to design a filter to remove 100% of the light and still pass the violet and ultraviolet (UV) light to the LIBS spectrometers. Therefore the Raman signal was left with this bump caused by the small amount of 532 nm light reflecting into the mast-to-body optical fiber. This artifact affects the identification of minerals whose primary

21699100, 2025, 11, Downloaded from https://agupubs.onlinelibrary.wiley.com/doi/10.1029/2025JE008943, Wiley Online Library on [18/11/2025]. See the Terms and Conditions (https://onlinelibrary.wiley.com/terms-and-conditions) on Wiley Online Library for rules of use; OA articles are governed by the applicable Creative Commons License

Raman features fall within this range, such as silicate-bearing minerals like feldspars or amorphous silica. Other igneous materials with features close to the artifacts, although not completely overlapped, such as olivine or pyroxene might also be affected, as well as other materials of interest such as perchlorates. Proper correction of this bump is therefore key for the interpretation and representation of data. The different strategies used for deconvoluting the sample signal from the fiber are discussed later in this work.

3.1. Optimizing the Acquisition Process

Because of the unique challenges of remote Raman analyses on Martian geological samples (dusty surfaces, small grain size, limited operational resources, etc.), tuning the acquisition parameters to optimize the Raman light collected by the instrument became a priority during the first months of operation on Mars. Tests and experiments on the Martian surface were conducted to understand the impact of different acquisition configurations, within the limits imposed by instrument operational parameters and available resources.

3.1.1. Number of Shots Versus Sample Points

It is widely recognized that enhancing the SNR of Raman spectra in standoff instruments such as SuperCam is most effectively achieved by increasing the number of laser shots. However, and as detailed in previous studies (Maurice et al., 2021; Wiens et al., 2021), the SuperCam Raman instrument relies on a passively cooled pulsed, frequency-doubled solid-state Nd:YAG laser for excitation, which is thus sensitive to heating during use, particularly in a low-density and poorly conductive atmosphere like that of Mars. The number of consecutive laser shots must therefore be carefully monitored, as these influence the laser's temperature and must be carefully controlled for instrument safety.

During operational activities, a typical SuperCam activity analyzes the Martian surface along a raster comprising up to 10 points on a designated sample. For SuperCam Raman, the nominal operational configuration involves 10 points, each with 100 laser shots. However, detailed analysis of SuperCam Raman spectra during early instrument operation on Mars suggested the need to explore the use of activities with increasing number of shots to maximize the resulting spectra SNR. These activities include 5- or 10-point rasters with 200 shots per point for Raman analysis. Notably, a more complex activity was implemented to substantially augment the number of shots to 400 per point, achieved by reallocating shots among points (i.e., performing two 200-shots consecutive acquisitions on the same point). This approach resulted in rasters featuring, for example, 10 points for LIBS and/or VISIR spectra, while limiting Raman analysis to only 4 points (typically, points 1, 4, 7, and 10 of the raster). Although operationally challenging due to the critical role of precise sample pointing and instrument safety, this approach has proven to be beneficial in terms of spectral quality, even with a reduced number of points dedicated to Raman analysis.

3.1.2. Number of Shots Versus Coadds

The SuperCam transmission spectrometer features the capability to integrate multiple shots and intensifier discharges in one detector readout, referred to as "coadding," as well as average different readouts during post-processing, termed "accumulating" (Wiens et al., 2021). Ground tests have demonstrated that the coadd-to-shots ratio, for a constant number of acquired shots, significantly impacts the SNR of the final spectra. This influence arises due to competition among various noise contributors from the detector, including readout noise, dark current, bias, and shot noise. These factors are, in turn, affected by environmental parameters on the Martian surface, especially temperature, but also radiation dose.

To determine the optimal number of coadds, a dedicated test was performed on the surface of Mars, analyzing the apatite calibration target. Using a total number of 100 laser shots, different data sets were acquired by coadding 1, 5, 10, and 20 laser shots in individual spectra. The laser is operated at the maximum repetition rate of 10 Hz, so the CCD exposure times for the latter three conditions are nearly 0.5, 1.0, and 2.0 s (the intensifier normally remains at 100 ns exposure times around each laser pulse). The resulting spectra sets were then averaged to create 100-shot spectra, each obtained with a different coadd configuration. The SNR was calculated for different shot counts, obtaining the evolution in terms of SNR increment with each new accumulation (see Manrique et al., 2024). The results indicated that a 10-coadd configuration provided the highest performance increase with each new accumulation.

21699100, 2025, 11, Downloaded from https://agupubs.onlinelibrary.wiley.com/doi/10.1029/2025JE008943, Wiley Online Library on [18/11/2025]. See the Terms and Conditions (https://onlinelibrary.wiley.com/terms-and-conditions) on Wiley Online Library for rules of use; OA articles are governed by the applicable Creative Commons License

Consequently, the 10-coadd setup has since been employed as the nominal configuration for the acquisition of Raman spectra with SuperCam.

3.1.3. Relative Focus Position

The SuperCam instrument employs an excitation with a footprint around ∼12 cm^2 spot (Maurice et al., 2021) that remains relatively constant in size for the working distance range of SuperCam. The Raman collection spot, however, varies between 1.5 and 8 mm for target distances between 2 and 7 m. Considering the instrument optical design, the variable Raman acquisition spot remains fully illuminated by the laser at all operational distances (Maurice et al., 2021). While this effect might limit the impact of inverse square law in the collected signal, potential misalignments between the collection and excitation, or more likely hot spots within the laser footprint, could affect the efficiency of the instrument at higher distances. In fact, concern for misalignment led to the design constraint of having this relatively large laser illumination area. Taking this into consideration, experimental validation on Mars with focus sweep analyses on the apatite and white paint samples of the calibration target was performed to study the efficacy of a slightly defocused collection strategy. Results indicated a slightly improved SNR (∼5%–10%) compared to the peak/fiber bump intensity ratio, showcasing the practical benefits of manipulating focus distance relative to the target distance for enhanced data quality during Raman spectroscopy operations on Mars. However, while the concept demonstrated potential improvements in controlled experiments on Mars the small performance increase would not be easy to test on geological samples, and we concluded that it would not justify the added complexity that would be introduced into the operational procedures.

3.1.4. Laser Energy and Discharge Rate

A close examination of the coadd-to-coadd variability in SuperCam Raman spectra revealed notable differences in band position, full width at half maximum (FWHM), and intensity of Raman features. While noise certainly contributes to this variability, potential modifications induced by changes in the excitation laser cannot be dismissed. The laser can operate at both low- (110 A) and high- (150 A) energy settings, and its discharge rate can be set to either 10 Hz (default) or 3 Hz.

Dedicated tests explored the influence of the shooting rate, indicating similar coadd-to-coadd variability in both cases. Likewise, altering the energy setup did not change the observed variability in terms of peak position, FWHM, or intensity among different coadds. Detailed analyses on this aspect are partially addressed by (Sharma, Olilla, Lopez-Reyes, et al., 2023) and will be fully covered in a dedicated manuscript. These findings suggest that the coadd-to-coadd variability is likely a result of the low SNR of the Raman spectra, where improvements through acquisition configurations might be limited, and thus emphasizing the importance of accumulating a sufficient number of laser shots per point to mitigate this effect.

3.1.5. Night-Time Acquisitions

During the execution of the first frost detection campaign on Mars with the Mars 2020 mission (Martínez et al., 2023), SuperCam Raman analysis were performed at both daytime and early morning (nighttime) on the same locations. While the results did not clearly indicate the presence of hydration or frost (Martínez et al., 2023), the analysis of the Raman data revealed a significant difference in signal quality. Specifically, the Raman spectra obtained at night showed a ∼4x improvement in SNR compared to those collected during the day (see Figure S2 in Supporting Information S1). Further analysis on the calibration target confirmed that the intensity of the Raman signal was correlated with temperature (Bernard et al., 2025). The conclusion drawn from these findings is that conducting Raman analysis at night or under colder conditions is advantageous, as it enhances the quality of the data. However, performing such nighttime analyses on a regular basis is challenging due to energy and operational constraints, though understanding this effect is important for optimizing future Raman measurements on Mars.

3.2. Optimizing the Raman Data Interpretation

The intrinsic characteristics of Raman spectra obtained by SuperCam on Mars, including the low SNR, the presence of spikes, or the collection optical fiber bump, necessitate careful and detailed data processing. This step is essential to enhance the detectability of features within the spectra and to maximize the scientific insights derived from the acquired data. This section describes the approaches adopted by the SuperCam Raman Working

21699100, 2025, 11, Downloaded from https://agupubs.onlinelibrary.wiley.com/doi/10.1029/2025JE008943, Wiley Online Library on [18/11/2025]. See the Terms and Conditions (https://onlinelibrary.wiley.com/terms-and-conditions) on Wiley Online Library for rules of use; OA articles are governed by the applicable Creative Commons License

Group and the broader SuperCam team to enhance the quality and thus interpretations based on SuperCam Raman data. Given the challenge of working with signals that are sometimes marginally above the noise level, the application of data processing is key to optimizing the detection and interpretation of subtle features in the Martian Raman spectra. The explored approaches encompass a range of techniques, including denoising algorithms, despiking methods, and debumping procedures, most of them included in the instrument automated data processing pipeline.

3.2.1. Data Processing Pipeline

The data processing pipeline to generate the SuperCam Raman spectra CDR files involves several critical steps to ensure the quality and reliability of the acquired data:

Saturation Check: The spectra are checked for intensity exceeding the threshold (64,500 counts), which is the limit for the digitizer. In case of saturation, a flag is activated in the header of the saturated spectrum file.

Non-persistent spike removal: Spikes present another challenge on Mars, where the absence of a protective magnetic field or atmosphere leads to a more frequent occurrence of these transient signals in spectra than on Earth. Additionally, the impact of low SNR further increases the presence of spikes, especially on dark-corrected spectra, where previously concealed signals become evident. To remove spikes, both dark spectra (acquired with no laser pulse) and active spectra (acquired with the laser on) undergo a sigma clipping process in the time domain (comparing the same pixel of subsequent coadds) to detect and eliminate non-persistent (transient) spikes. This algorithm, widely used in astronomy, iteratively identifies points that deviate from the median value by a specified number of standard deviations and substitutes them with the median value. Typically, cosmic rays impacting the detector appear as sharp peaks in one (or a reduced number) of coadds. These spikes are very efficiently removed with this algorithm (see example in Figure S3 in Supporting Information S1).

Dark Subtraction: The mean of all the acquired dark spectra is calculated and subtracted from every active spectrum to correct the intrinsic instrument and detector noise.

Statistics calculation: The mean, median and standard deviation spectra are calculated from all the coadds acquired on a sample point.

Spectral stitching: Raman spectra are obtained using three tracks on the detector of the instrument transmission spectrometer (Wiens et al., 2021). The three tracks are stitched together selecting each track pixels based on predefined spectral positions, which provides optimal alignment of the tracks (Anderson et al., 2021). Since this optimization was based on LIBS data (with low baseline), the resulting stitching could not be optimal for spectra with significant background signal, as observed in some Raman or luminescence spectra. The stitching process is done for coadds and statistics spectra.

Denoising: Spectra noise is reduced based on a wavelet transform denoising process, inherited from ChemCam and adapted for SuperCam (Anderson et al., 2021). This technique has demonstrated effective noise reduction in both Raman and LIBS data. This is done for coadds and statistics spectra.

Instrument Response Function (IRF) Correction: The spectra are calibrated in intensity with the aim of correcting the differences in sensitivity across the different regions of the detector (Legett et al., 2022). This applies to coadds and statistics spectra.

Persistent spike removal: Spikes with longer persistence (appearing in many or all coadds in an acquisition) are also observed on the SuperCam Raman data. They can be produced hot pixels on the detector or intensifier). This kind of persistent spikes cannot be efficiently corrected by sigma clipping in the time domain, as it can be observed on the median spectrum (which means it can be observed on more than half of the coadds). However, applying the process in the spectral (wavelength) domain can effectively help reduce many of the high-intensity persistent spikes (see example in Figure S3 in Supporting Information S1). This process is applied to the mean and median spectra.

3.2.1.1. Post-Processing of the Data: Fiber Bump Correction

The SuperCam Raman spectra "fiber bump" is shown in Figure S1 in Supporting Information S1. The observed correlation of the spectral background and fiber-induced signal with both distance and the albedo of the analyzed

21699100, 2025, 11, Downloaded from https://agupubs.onlinelibrary.wiley.com/doi/10.1029/2025JE008943, Wiley Online Library on [18/11/2025]. See the Terms and Conditions (https://onlinelibrary.wiley.com/terms-and-conditions) on Wiley Online Library for rules of use; OA articles are governed by the applicable Creative Commons License

targets using both Raman and reflectance techniques (see Kelly et al. (2023), and Figure S4 in Supporting Information S1), supports the conclusions that this phenomenon is indeed compatible with light generated at the instrument by the backscattered laser light.

Various strategies for the correction of this artifact have been explored (Manrique et al., 2022). The fiber bump was experimentally characterized in the laboratory by obtaining Raman spectra of a spare sample of the instrument fiber. This reference is then compared to and/or subtracted from the acquired spectra, proving to be especially effective when correcting uncalibrated (EDR) data. Another method relies on Independent Component Analysis (Clavé et al., 2024d) to extract components associated with actual features observed on Mars on the calibrated products, providing a reference of the fiber signature for subtraction on the CDRs. To avoid including additional noise during correction, the modeled fiber spectra were deconvoluted to individual Voigt profile bands. This is particularly suited for correction of the fiber bump on clean (CDR) spectra.

An alternative method for correcting the fiber-induced signal on the Raman spectra involves subtracting spectra of the same sample lacking the features of interest (Sharma, Ollila, Madariaga, et al., 2023). This is applicable to any sample, but has proven particularly efficient for the correction of spectra from veins, where the Raman signal of the mineral is well above the spectral noise. Subtracting denoised spectra collected outside the vein effectively removes the fiber bump without compromising the signals from the vein.

As these processes are challenging for automated application, the de-bumping process needs to be applied with care for proper representation of the Raman data.

3.2.2. Other Strategies to Process SuperCam Raman Data

In addition to processing steps aimed at correcting instrumental artifacts, other strategies to improve spectral quality have been employed to improve the overall detection capabilities of SuperCam Raman by considering in-point or in-sample averaging approaches, as described below.

Mean versus median: Since SuperCam provides multiple spectra (coadds) on a given point, the choice between using mean or median spectra as the final product is a critical consideration. While the median is more robust against spikes, the mean generally provides better SNR. After the successful implementation of despiking algorithms into the pipeline, Raman data are analyzed based on the mean, prioritizing improved SNR of the data.

Coadd-to-Coadd Analysis: When Raman features are weak and close to the noise level, it is critical to assess the validity of the detection. If uncertain about a specific feature, one can study the individual coadds on the same point. If the feature consistently appears across most of the coadds, then it is considered a detection, since noise will randomly change among coadds. If the feature is not consistent, then the following strategies are considered.

Cross-Technique correlation: Interpretations are strengthened by cross-referencing with other analytical techniques within SuperCam. When Raman data alone don't enable us to confirm a mineral detection with enough confidence, LIBS and VISIR results can help, especially when they also show evidence of the suspected mineral phase. The lack of confirmation with another technique is however not sufficient to dismiss a potential Raman detection altogether, considering the differences in analytical footprints and sensitivities of these different techniques.

Averaging spectra in different points: The use of the other SuperCam techniques has facilitated additional robust and honest approaches to enhance Raman detections by averaging spectra obtained in different sample points, for example, averaging spectra obtained in points showing similar textures in the RMI images or similar VISIR signatures. Additionally, blindly averaging all the spectra obtained on a sample, even from different sols, has contributed to successful observations. This approach limits the capability of identifying inter-point mineral diversity, but it sometimes allows identifying the major mineral present in the sample.

The SuperCam team is committed to providing unbiased and robust interpretations of the data. As such, cherry-picking spectra from a raster or selectively choosing and averaging coadds displaying only the desired features on the Raman data has not been considered an acceptable approach in the analysis of SuperCam Raman spectra. Indeed, especially for low-SNR spectra where features are unclear, selecting and averaging only spectra with potential features would most likely yield results that could be biased by the spectra selection process.

21699100, 2025, 11, Downloaded from https://agupubs.onlinelibrary.wiley.com/doi/10.1029/2025JE008943, Wiley Online Library on [18/11/2025]. See the Terms and Conditions (https://onlinelibrary.wiley.com/terms-and-conditions) on Wiley Online Library for rules of use; OA articles are governed by the applicable Creative Commons License

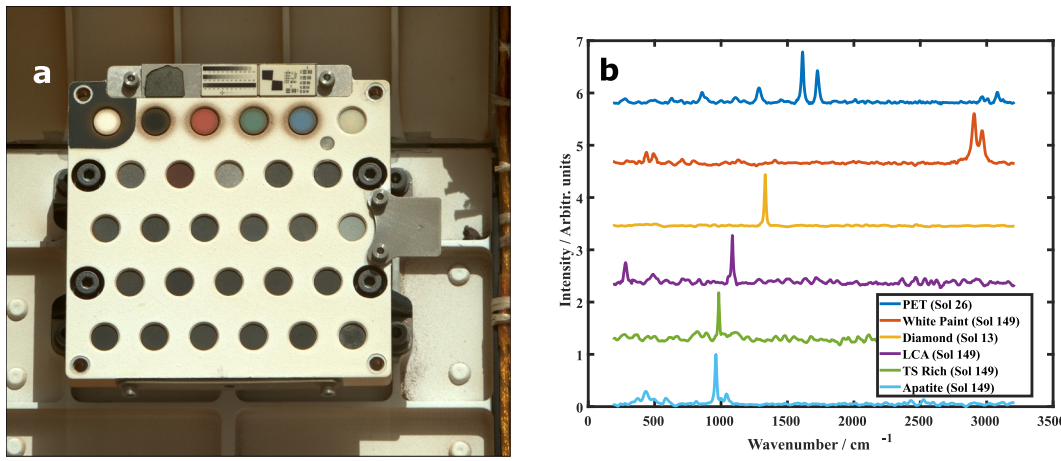

Figure 1. (a) SuperCam calibration target (SCCT) soon after its arrival on mars. (b) Examples of Raman spectra acquired on the SCCT.

4. 1,000 Sols of SuperCam Raman Observations on Mars

This section delves into the detections performed by SuperCam during the first 1,000 sols of operations on Mars, beginning with a short summary of the analyses performed on the SCCT. Subsequently, the focus shifts to the Raman data acquired for the exploration of geological samples within the Jezero Crater.

4.1. Analyses Performed on the SuperCam Calibration Targets

4.1.1. Diamond Target

The SCCT (Cousin et al., 2022; Madariaga et al., 2022; Manrique et al., 2020) features a diamond target instrumental in verifying the SuperCam Raman performance and calibration, considering the stable nature of its Raman scattering. On sol 13 of Mars operations, SuperCam analyzed this 8-mm diameter synthetic diamond glued to the SCCT aluminum holder, resulting in the first-ever Raman spectrum acquired beyond Earth (see Figure 1) (Beyssac et al., 2021). The spectrum clearly shows the Raman scattering of the diamond at 1,332 cm^{-1}, albeit with an elevated background due to the fluorescence of the glue securing the diamond to the holder (Manrique et al., 2020).

Subsequent analyses of the diamond target, analyzed every 50–60 sols since sol 239 (a total of 16 observations during the first 1,000 sols), have shown variations attributed to environmental factors affecting the glue, such as surface UV radiation, but the Raman signal of the Diamond target did not change with time. The lack of evolution of the Raman signal shows there is no evident evolution of the instrument performance. A more detailed exploration of this phenomenon is described by Bernard et al. (2025).

4.1.2. Organic Target

The SCCTs incorporate a dedicated highly crystalline Polyethylene Terephthalate (PET, Ertalyte®, $(C_{10}H_8O_4)_n$) target dedicated to the SuperCam Raman. This material, proposed as a calibrating material for other Raman instruments for planetary exploration (Lopez-Reyes et al., 2018; Moral et al., 2023), exhibits a number of astrobiologically relevant Raman features: 633 cm^{-1} (C−C−C in plane bending), 859 cm^{-1} (left ethylene glycol), 1,095 cm^{-1} (C−C bonds), 1,120 cm^{-1} (ester C(O)−O), 1,288 cm^{-1} (ring C−H bending in-plane), 1,612 cm^{-1} (ring mode), 1,726 cm^{-1} (stretching C = O), 2966 cm^{-1} (methylene groups adjacent to oxygen atoms) and 3,083 cm^{-1} (aromatic C−H bond) (see Figure 1). Such Raman features are typical of organic compounds expected to be found in ancient rocks (Bernard & Papineau, 2014). In addition to ensuring that the SuperCam Raman was capable of detecting organic polymers at the surface of Mars, the Ertalyte target has allowed conducting an in situ 1,000-sols-long aging experiment under actual Martian conditions: The Ertalyte target has been periodically measured with a cadence of 50–60 sols using Raman throughout the mission, allowing documenting the effect of UV radiation (Bernard et al., 2025). Although it was white at landing, the Ertalyte target has turned brown with time, while its Raman signal has significantly changed, as a result of an increase in the concentration of electronic

21699100, 2025, 11, Downloaded from https://agupubs.onlinelibrary.wiley.com/doi/10.1029/2025JE008943, Wiley Online Library on [18/11/2025]. See the Terms and Conditions (https://onlinelibrary.wiley.com/terms-and-conditions) on Wiley Online Library for rules of use; OA articles are governed by the applicable Creative Commons License

defects and/or radicals, responsible for a modification of the shape of the background and a reduction of the contribution of the Raman signature of pristine Ertalyte to the total signal. The increase of daily temperature in the Jezero crater when Mars was approaching its perihelion likely triggered a second stage of UV-induced degradation, increasing the volume of Ertalyte damaged by UV, further limiting the contribution of pristine Ertalyte to the total signal (Bernard et al., 2025).

4.1.3. Calcite, Sulfur-Rich and Apatite Targets

The great majority of the SCCTs are dedicated to the calibration of the LIBS technique. Most of these were manufactured by a sintering process of mineralogic materials and are referenced and detailed by Cousin et al. (2022). Despite the structural changes induced by the sintering process (mostly amorphization of the mineral phases (Montagnac et al., 2018)), several of the samples maintain enough structural integrity to be detectable by Raman, especially the samples Calcite (LCA–calcium carbonate with formula $CaCO_3$), Apatite (TAPAG–a synthetic fluorinated and chlorinated hydroxy-apatite whose general formula is $Ca_5(PO_4)3(OH,F,Cl)$), and the Basalt + Sulfate mix (TSRich–a mixture of 30% of the USGS BHVO-2 standard and 70% of arcanite, the potassium sulfate with formula K_2SO_4). The SuperCam Raman analysis of these samples presents discernible Raman spectra as shown in Figure 1. These samples have been analyzed a few times throughout the first 1,000 sols of the mission (sols 149, 636, 836, 888, 936 for LCA; sols 51, 55, 60, 149, 352, 484, 606, 636, 715, 836, 888, 936 for TAPAG; sols 149, 836, 888, 936 for TSRich) to characterize and assess the instrument performance, and monitor potential degradation of the instrument or the samples. LCA and TSRich samples showed a decrease of the Raman signal and continuum intensity between the first two observations (far apart, unfortunately), but have kept stable since then. TAPAG, on the other hand, shows a systematic decrease of signal intensity and SNR of the nu1 band, inversely correlated to the increasing spectral background. This degradation effect is attributed to UV irradiation of the sample, as detailed in (Clavé, Beyssac, et al., 2024), and is supported by previous laboratory work (Royer et al., 2024).

4.1.4. Paint of the SCCT Holder

The SCCTs include an additional material that can be analyzed by SuperCam Raman: the paint of the calibration target holder. This material can be safely measured with the SuperCam Raman, leading to spectra exhibiting two intense Raman features (2,905 and 2,965 cm^{-1}, Figure 1). The Raman data collected on the paint of the SCCT holder throughout the mission showed that it did not suffer from UV radiation damage (Bernard et al., 2025) making it a reference material ensuring that the SuperCam Raman instrument has worked in an optimal configuration since the landing of Perseverance. However, these showed how the signal intensity of SuperCam Raman was correlated with local ambient temperature (Bernard et al., 2025).

4.2. Analyses Performed on Geological Targets

The following section compiles the Raman mineral detections conducted by SuperCam over the first 1,000 sols of the mission, classified by mineral type and divided by mission campaign. These detections are graphically compiled in Figure 2, and summarized in Table 1. Raman mineral detections are also provided in the (SuperCam Raman Mineral detections table compiled in NASA's Planetary Data System repository, n.d.).

4.2.1. Olivine

Olivine is a neso-silicate mineral ($(Mg,Fe)_2SiO_4$) featuring a diagnostic doublet peak in the Raman spectrum at ~820 and ~850 cm^{-1} from the coupled symmetric and asymmetric stretching vibrational modes of the SiO_4 tetrahedra (Chopelas, 1991; Lam et al., 1990). The variable presence of cations (mainly Fe and Mg) can modify the position of the doublet peaks, which can be used to define the Fe/Mg content present on the sample (Kuebler et al., 2006). This mineral has been observed by SuperCam in many places at Jezero.

4.2.1.1. Crater Floor

SuperCam Raman successfully identified these minerals during the Séítah traverse, on abraded rocks and natural surfaces both, on a number of samples: Garde, Penne, Brac, Castellet, Dourbes and Quartier (see Figure 3).

21699100, 2025, 11, Downloaded from https://agupubs.onlinelibrary.wiley.com/doi/10.1029/2025JE008943, Wiley Online Library on [18/11/2025]. See the Terms and Conditions (https://onlinelibrary.wiley.com/terms-and-conditions) on Wiley Online Library for rules of use; OA articles are governed by the applicable Creative Commons License

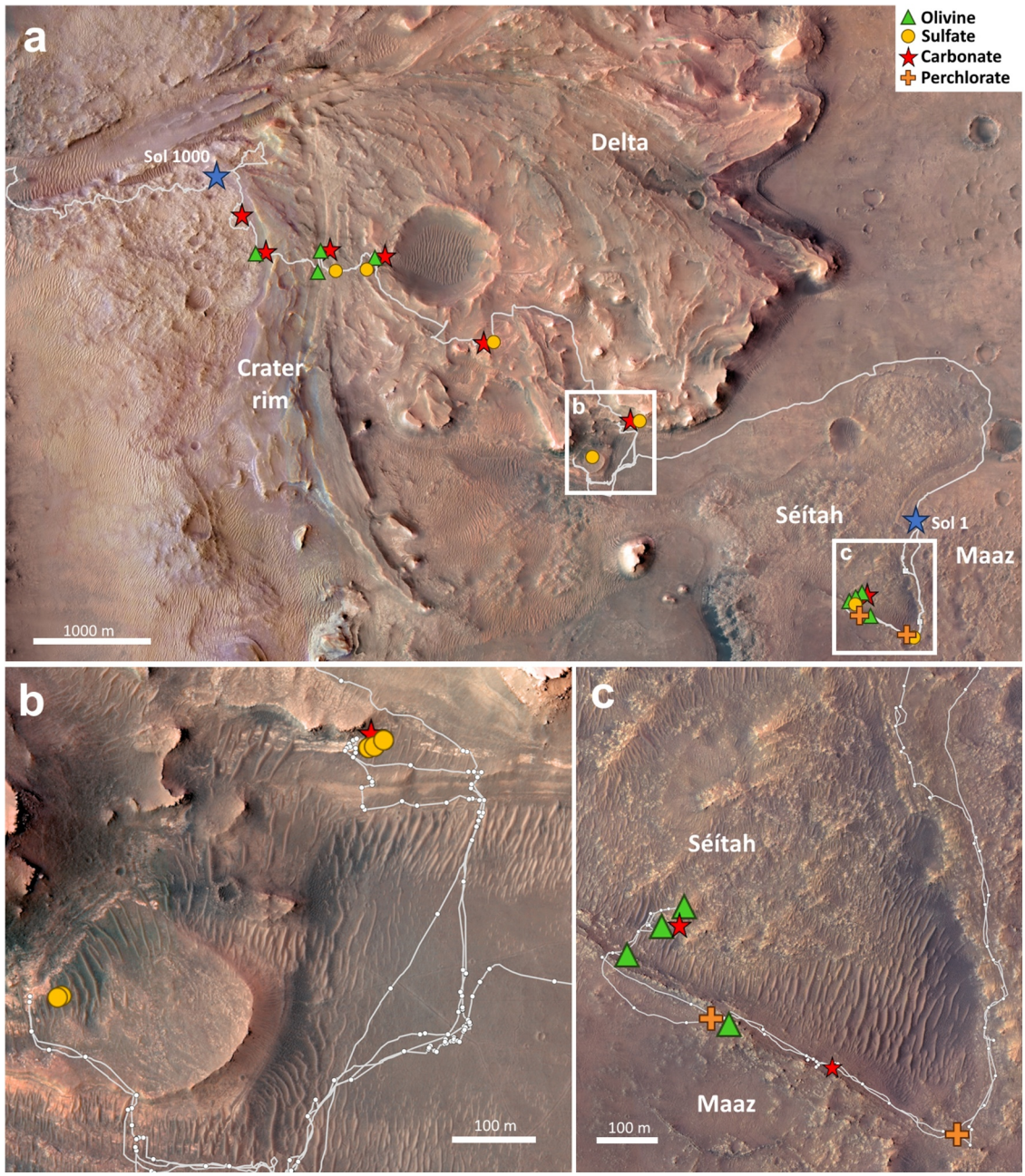

Figure 2. Map of detections by Perseverance with SuperCam Raman during the first 1,000 sols of the mission (a), with zoom on the delta front (b) and Séítah (c) regions.

Garde is an abraded patch analyzed by SuperCam Raman on sols 207, 209, and 210, acquiring a total of 27 points on the patch (three rasters of 3 × 3 points) with 100 shots (10 coadds of 10 shots) per point. The presence of olivine is ubiquitous on the patch, with variable spectral quality among points, but relatively high when averaging the spectra in all points. Other abraded patches analyzed by Raman, which detected potential olivine on the crater floor were Dourbes on sols 259 (1 × 9 raster, 10 coadds), 268 (1 × 10 raster with 4 Raman points, 200 shots −20 coadds of 10 shots– each) and 278 (1 × 5 raster with 3 Raman points, 20 coadds), and Quartier on sols 295 (1 × 10 raster, 10 coadds) and 303 (1 × 5 raster with 3 Raman points, 20 coadds). The results on Dourbes revealed the presence of olivine in most of the points, exhibiting acceptable quality in several points, showing both characteristic peaks of the doublet at around 820 and 850 cm^{-1}. In contrast, Quartier spectra primarily displayed an elevation of the intensity above the fiber bump feature around 800 cm^{-1}, with more reliable signals of olivine in one point and potential hints on another three, overall indicating a challenging olivine detection in Quartier. This

21699100, 2025, 11, Downloaded from https://agupubs.onlinelibrary.wiley.com/doi/10.1029/2025JE008943, Wiley Online Library on [18/11/2025]. See the Terms and Conditions (https://onlinelibrary.wiley.com/terms-and-conditions) on Wiley Online Library for rules of use; OA articles are governed by the applicable Creative Commons License

Table 1
Summary of Detections by SuperCam Raman During the First 1,000 Sols of the Mission

	Olivine				Sulfate				Carbonate				Perchlorate			
Region	Unit/Outcrop	Sample	Type	Sols	Unit	Sample	Type	Sols	Unit	Sample	Type	Sols	Unit	Sample	Type	Sols
Crater floor					Maaz	Guillaumes	Abraded patch	162					Maaz	Guillaumes	Abraded patch	162
														Bellegarde		188
	Séítah	Garde	Abraded patch	207, 209, 210	Séítah	Quartier		297	Séítah	Garde	Abraded patch	209	Séítah	Quartier		303
		Dourbes		259, 268, 278												
		Quartier		295, 303												
		Penne	Natural surface	211												
		Brac		246, 247												
		Castellet		248												
Delta front					Hogwallow Flats	Reids Gap	Light-toned vein	466	Lower Rockytop	Thornton Gap	Abraded patch	486, 491, 493, 498				
						Dovel Mountain		512								
						Mill Prong		517								
						Berry Hollow	Abraded patch	518								
					Yori Pass	Kupreanof Strait	Light-toned vein	620								
						Uganik Island	Abraded patch	619								
Delta Upper fan	Curvilinear	Solva	Abraded patch	748, 751	Curvilinear	Solva	Abraded patch	751	Curvilinear	Solva	Abraded patch	748, 751				
										Solitude Lake		783				
	Blocky	Ouzel Falls		791, 792, 803					Blocky	Ouzel Falls		803				
	Lobe/Trough m	Gabletop Mountain		881	Lobe/ Trough m	Thunderbolt Peak	Abraded patch	896	Lobe/ Trough m	Gabletop_Mountain_88		881				
		Thunderbolt Peak	Natural surface, GDRT	890												
	Olivine-rich Boulder	Mount Chapin	Natural surface	848	Pyroxene-rich Boulder in Mount Meeker	Dragons Egg		862								
		Lake Haiyaha	Abraded patch	853												
Delta Margin	Hans Amundsen Memorial Workspace	Amherst Point	Abraded patch	922, 925					Hans Amundsen Memorial Workspace	Amherst Point	Abraded patch	925				
					Turquoise Bay outcrop	Bills Bay	Abraded patch	940	Turquoise Bay outcrop	Bills Bay		940, 941				

21699100, 2025, 11, Downloaded from https://agupubs.onlinelibrary.wiley.com/doi/10.1029/2025JE008943, Wiley Online Library on [18/11/2025]. See the Terms and Conditions (https://onlinelibrary.wiley.com/terms-and-conditions) on Wiley Online Library for rules of use; OA articles are governed by the applicable Creative Commons License

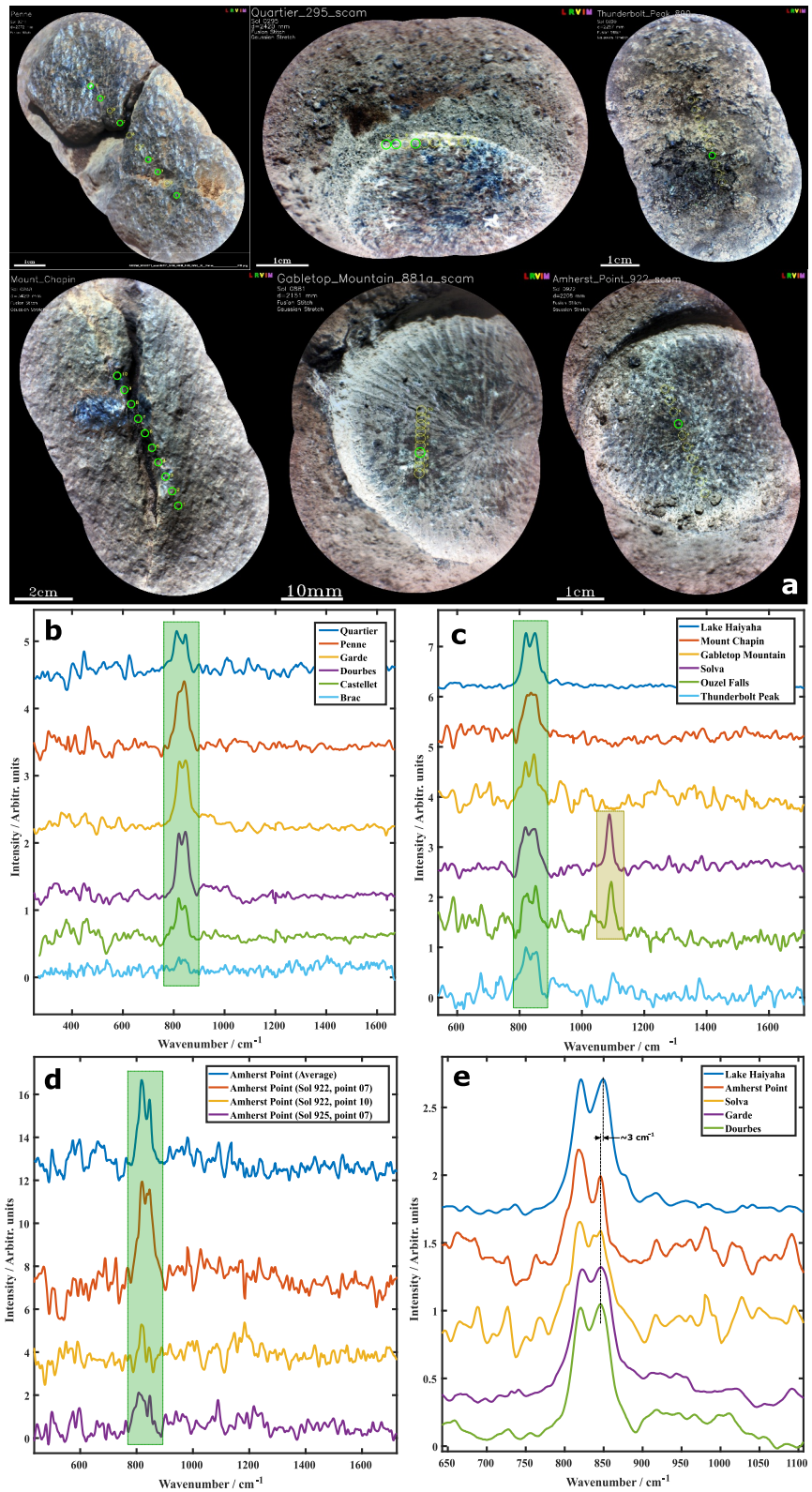

Figure 3.

21699100, 2025, 11, Downloaded from https://agupubs.onlinelibrary.wiley.com/doi/10.1029/2025JE008943, Wiley Online Library on [18/11/2025]. See the Terms and Conditions (https://onlinelibrary.wiley.com/terms-and-conditions) on Wiley Online Library for rules of use; OA articles are governed by the applicable Creative Commons License

difference is explained by the different protolith of Quartier, which has a smaller grain size (Beyssac et al., 2023), while also showing more alteration (more frequent presence of phyllosilicates and carbonates) (Beyssac et al., 2023; Clavé, Benzerara, et al., 2023).

The analyses of natural surfaces on Séítah by SuperCam Raman provided olivine detections in targets Penne on sol 211 (1 × 10 raster, 10 coadds), Brac on sols 246 (1 × 10 raster, 10 coadds) and 247 (1 × 2 Raman raster, 20 coadds), and Castellet on sol 248 (1 × 10 raster, 10 coadds). In the case of Penne, a few points displayed reasonable spectral quality, albeit with difficulties resolving the doublet. Castellet, on the other hand, exhibited low SNR olivine signals in most points. Brac analysis was limited in both detection points (only two) and SNR (very low), again only inferring the olivine presence due to an elevation above the fiber bump in the olivine region. Overall, Raman features of olivine appeared consistently weaker on natural surfaces compared to abraded patches.

4.2.1.2. Western Fan

During the exploration of the delta, olivine features were notably absent from SuperCam Raman analyses in the fan front area, which could be partly explained by higher degrees of alteration observed by SuperCam's IR spectrometer in this area (Dehouck, Forni, et al., 2024), and the very small grain size found in the rocks of the area. In contrast, olivine was identified in several locations on the upper fan, including three abraded patches (Solva, Ouzel Falls, and Gabletop Mountain) and a natural surface (Thunderbolt Peak). In addition to these bedrock targets, olivine was also identified in boulders deposited on top of the fan, including again both natural and abraded surfaces (Mount Chapin and Lake Haiyaha). Spectra are shown in Figure 3.

The Solva abraded patch, situated in the curvilinear unit of the fan, was analyzed by SuperCam Raman on sols 748 and 751, by a 1 × 10 raster with 4 Raman points, 400 shots (40 coadds of 10 shots) each. The results show a diverse mineralogy with olivines, carbonates, and sulfate. Olivine was identified in 5 out of the 8 analyzed points, often co-occurring with carbonate.

The Ouzel Falls abraded patch analysis on the blocky unit of the fan was carried out on sols 791 and 792 (1 × 10 rasters with 4 Raman points, 40 coadds each), and sol 803 (1 × 5 raster, three Raman points, 40 coadds). Weak olivine signatures were detected by Raman in several points of this abraded patch, marked by an elevated signature in the olivine region above the fiber bump. Gabletop Mountain is an abraded patch on the Dream Lake outcrop of the Lobe/Trough unit. It was analyzed on sol 881 by means of a 1 × 10 raster with four Raman points, 40 coadds each, revealing the presence of both olivine and carbonate. Additionally, luminescence spectra acquired by SuperCam on the same sol–luminescence spectra use a longer integration time than Raman observations– unexpectedly captured the Raman signal of olivines. Thunderbolt Peak (sol 890) is a natural surface on the Willow Park outcrop of the Lobe/Trough m unit, in which dust was blown out by the Gas Dust Removal Tool (Farley et al., 2020). The Raman analysis of this surface (1 × 10 raster with four Raman points, 40 coadds each) also exhibited signals of olivine in one point.

The analysis on boulders (Beyssac et al., 2024) included a natural surface in Mount Chapin (sol 848, 1 × 10 raster, 10 coadds) with clear olivine signals, however the very noisy nature of the spectra precluded the olivine doublet resolution. Additionally, the Lake Haiyaha abraded patch, analyzed on sol 853 using a 1 × 10 raster with four Raman points, 40 coadds, displayed the best olivine signal acquired by SuperCam Raman during the mission during the first 1,000 sols.

4.2.1.3. Margin Unit

The Margin unit data included in this study (sols 910–1,000), revealed spectra of olivines in the Amherst Point abraded patch at the Hans Amundsen Memorial Workspace. These spectra were acquired on sols 922 and 925 using 1 × 10 rasters with 4 Raman points, 40 coadds each. Although the spectra are relatively low in quality

Figure 3. Olivine detections performed by SuperCam Raman on the first 1,000 sols. (a) Close-up images of analyzed points on several abraded patches and natural surfaces with olivine detections (color is gaussian stretched). Points of detection indicated in green. (b, c, d) Raman spectra with olivine signals obtained for each sample (average spectra of all olivine detections in the sample, highlighted in green) in Séítah (b), in the delta (c) and the Margin (d). Carbonate detections in the delta are shown in light brown (c). (e) Comparison of the ~850 cm^{-1} (DB2) olivine band at several locations, indicating a higher Fo# on the Lake Haiyaha upper fan boulder compared to other units.

21699100, 2025, 11, Downloaded from https://agupubs.onlinelibrary.wiley.com/doi/10.1029/2025JE008943, Wiley Online Library on [18/11/2025]. See the Terms and Conditions (https://onlinelibrary.wiley.com/terms-and-conditions) on Wiley Online Library for rules of use; OA articles are governed by the applicable Creative Commons License

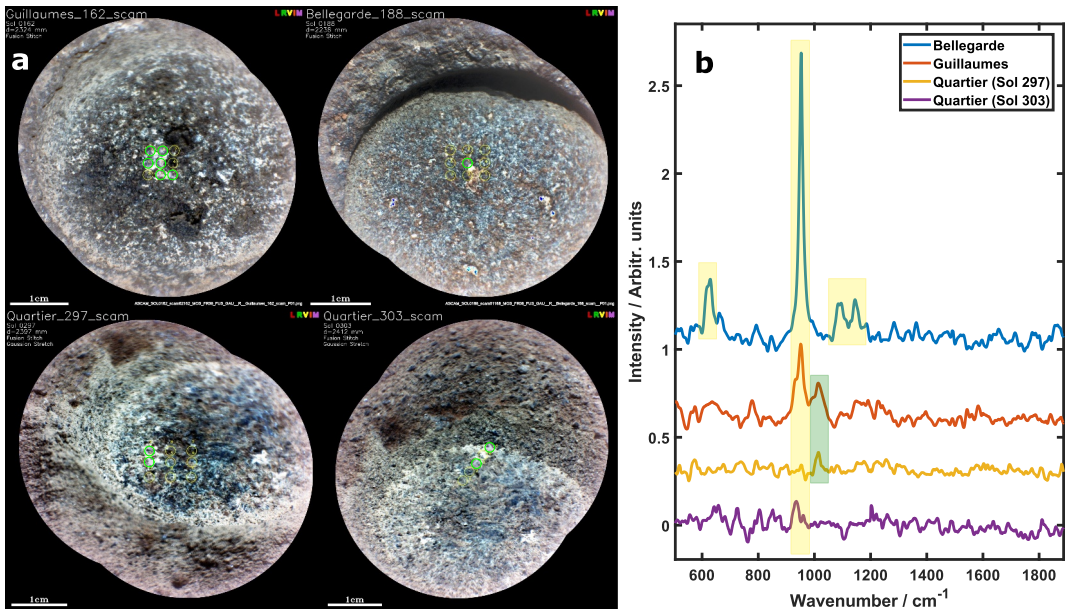

Figure 4. Perchlorate and sulfate detections performed by SuperCam Raman during the crater floor campaign. (a) Close-up images of the Guillaumes, Bellegard and Quartier (sols 297 and 303) abraded patches. Color is gaussian stretched. Points with Raman detections highlighted in green. (b) Spectra displaying perchlorate (yellow) and sulfate (green) features by Raman. Bellegarde (point 5) and Guillaumes (average of spectra in white material) exhibit anhydrous Na-perchlorate. Quartier 303 average spectra on white material displays a weak feature compatible with (possibly Mg) perchlorate. Guillaumes and Quartier 297 also exhibit potential Ca/Mg sulfate features.

spectra when detected alongside carbonates, certain points with no carbonate co-existence display better olivine signal SNR. Later Margin Unit data are not included in this study.

4.2.2. Perchlorates

Perchlorates are a group of salts containing the perchlorate ion (ClO^-) and are characterized by distinct peaks in their Raman spectra, the most intense corresponding to the stretching vibrations of the Cl-O bonds in the tetrahedral perchlorate anion, typically around ~930 and ~980 cm^{-1}. The presence of different cations (such as Na^+, K^+, or Mg^{2+}) or hydration levels can influence the position of these peaks, which can be used to identify the specific type of perchlorate and its composition in a sample.

4.2.2.1. Crater Floor

The Bellegarde abraded patch (sol 188) was analyzed using a 1 × 10 raster with 100 shots each, providing a high-quality sodium perchlorate spectrum on point 5, with features at 954, 635, 1,099, and 1,153 cm^{-1} (Wiens et al., 2022). Supported by this detection and the elevated chlorine identified by SuperCam LIBS, the Guillaumes abrasion patch analysis (sol 162, 1 × 10 raster with 100 shots) suggested elevated Raman features in the ~950 cm^{-1} region, also indicating the detection of perchlorate. Quartier (sol 303, 1 × 5 raster with 3 Raman points, 400 shots) presents a white spot on point 4 of the raster, which was not analyzed by Raman. However, the spectra could be showing traces of Mg-perchlorate with a signal at ~935 cm^{-1} on the points partially overlapping the white material (#3 and #5). See Figure 4.

4.2.3. Sulfates

Sulfates are a class of minerals that contain the sulfate ion (SO^{2-}) and are characterized by prominent Raman peaks typically around ~980 and ~1,050 cm^{-1}, corresponding to the symmetric and asymmetric stretching vibrations of the sulfate ion. The position and intensity of these peaks can vary depending on the type of cation (such as Ca^{2+}, Mg^{2+}, or Na^+) associated with the sulfate, allowing for the identification and characterization of different sulfate species by their Raman spectra. One important example is calcium sulfates, which can occur in different hydration states that can be readily identified by Raman spectroscopy. These include gypsum

21699100, 2025, 11, Downloaded from https://agupubs.onlinelibrary.wiley.com/doi/10.1029/2025JE008943, Wiley Online Library on [18/11/2025]. See the Terms and Conditions (https://onlinelibrary.wiley.com/terms-and-conditions) on Wiley Online Library for rules of use; OA articles are governed by the applicable Creative Commons License

($CaSO_4 \cdot 2H_2O$), bassanite ($CaSO_4 \cdot 0.5H_2O$), and anhydrite ($CaSO_4$). Anhydrite itself is a polymorph that can occur in three distinct structural forms with different properties (Prieto-Taboada et al., 2014): type I (cubic structure, insoluble, stable), type II (orthorhombic structure, insoluble, stable), and type III (hexagonal structure, soluble, metastable). These polymorphs can also be distinguished by Raman spectroscopy as shown by Prieto-Taboada et al. (2014).

4.2.3.1. Crater Floor

The SuperCam measurements performed on the crater floor led to a few detections of Ca/Mg sulfates. This was observed in both the Guillaumes and Quartier abraded patches through VISIR reflectance and LIBS analyses (Mandon et al., 2023; Wiens et al., 2022). Supported by these detections, the Raman spectra were further examined for sulfate features. Indeed, averaging the spectra acquired over a white region of each abraded patch showed elevated signatures in the sulfate region for both Guillaumes (sol 162, 1 × 10 raster with 100 shots) and Quartier (sol 297, 1 × 10 raster with 100 shots) (Figure 4). While these features might be subtle in Raman data alone, the congruence of these features with results from the other SuperCam techniques supports the overall interpretation.

The analysis performed by Mars 2020 on the Jezero western fan have led to the identification of several occurrences of white material observed on natural exhumations and light-toned veins on rocks (Nachon et al., 2023, Nachon, Lopez-Reyes, et al., 2024), or in mostly white spots on abraded patches.

4.2.3.2. Western Fan–Light-Toned Veins on the Fan Front

The SuperCam Raman examination of light-toned veins featuring sulfates first yielded results in Reids Gap, a cm-wide light-toned vein on the Hogwallow flats outcrop at the fan front (Figure 5). Analyzed on sol 466 (1 × 5 raster with three Raman points, 400 shots each), the results presented a highly distinct detection of Anhydrite Type II (orthorhombic) polymorph (Lopez- Reyes et al., 2023). Indeed, all the anhydrite type II Raman features (Prieto-Taboada et al., 2014) were identified on the Reids Gap spectra (Figure 5), these spectra representing the strongest detections achieved by SuperCam Raman over the first 1,000 sols of the mission, obtaining peaks more than 1,500 counts high. Additionally, the spectra on Reids Gap showed a doublet at ~800,

~819 cm^{-1} potentially related with Nd^{3+} luminescence, though this hypothesis is currently under study.

The Reids Gap detection is unambiguous from the Raman data and in agreement with Ca sulfate detections by LIBS and VISIR. However, the anhydrous nature of the sulfate needs to be specifically addressed, since VISIR shows evidence of hydration on these samples (Lopez-Reyes et al., 2023). Considering the unambiguous detection by Raman and the high sensitivity of IR to the presence of water, the hypothesis is that the ~1.4 and ~1.9 μm absorption bands observed in the VISIR spectra of Reids Gap are related to a minor presence of OH and H_2O, either molecular in trace amounts or adsorbed on the sample surface, but this hydration cannot be considered structural water of the sulfate due to the lack of the Raman hydration peak (Lopez- Reyes et al., 2023).

Additional light-toned veins with sulfate detections analyzed by SuperCam (Nachon et al., 2023, Nachon, Lopez-Reyes, et al., 2024) include Dovel Mountain (sol 512, 1 × 10 raster with 100 shots) and Mill Prong (sol 517, 1 × 5 raster with three Raman points, 400 shots each) in the Hogwallow Flats member, as well as Kupreanof Strait in the Yori Pass member, which is considered as a lateral equivalent of Hogwallow Flats (sol 620, 1 × 10 raster with 4 Raman points, 400 shots each). The analysis of these also showed clear detections of anhydrite, allowing again to narrow it down to anhydrite type II on Mill Prong. Other examinations of surface disturbed white material such as Lands Run in Hogwallow Flats provided hints of anhydrite, however very weak due to the substantial working distance (~7 m) and are therefore not considered in this work.

4.2.3.3. Western Fan–Abraded Patches

The analysis of abraded patches on the fan front also revealed several sulfate detections in the bedrock. In Berry Hollow (sol 518, 1 × 5 raster with three Raman points, 400 shots) potential very weak signatures of sulfate were observed as a slight elevation above the bump-corrected average of the spectra. More interestingly, this abraded patch exhibited a distinctive and elevated continuum signal on the Raman spectra, the origin of which is currently under investigation (Clavé, Beyssac, et al., 2023). A similar elevated background was also observed in other

21699100, 2025, 11, Downloaded from https://agupubs.onlinelibrary.wiley.com/doi/10.1029/2025JE008943, Wiley Online Library on [18/11/2025]. See the Terms and Conditions (https://onlinelibrary.wiley.com/terms-and-conditions) on Wiley Online Library for rules of use; OA articles are governed by the applicable Creative Commons License

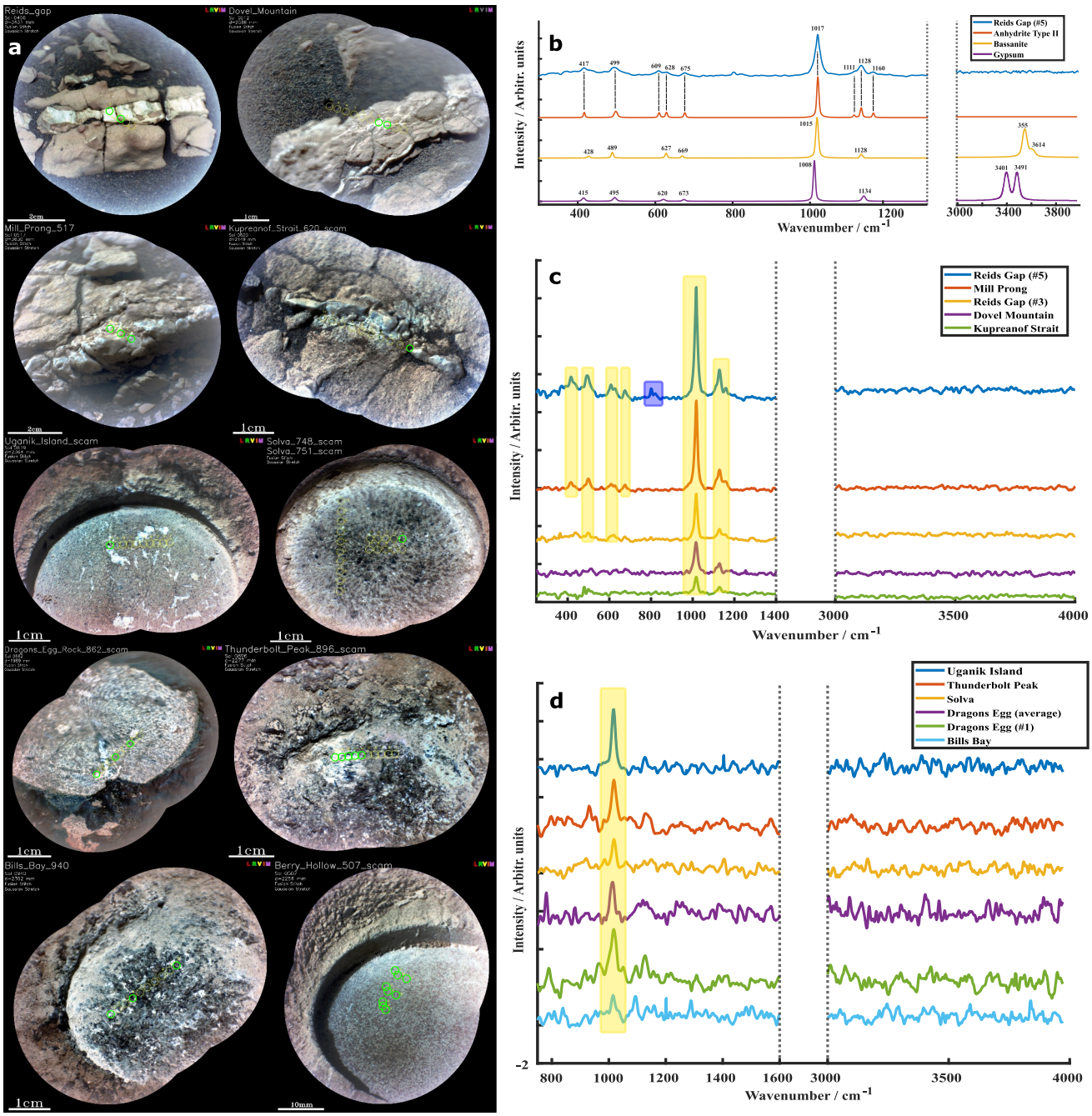

Figure 5. Sulfate detections with SuperCam Raman during the first 1,000 sols of the mission on the Jezero Delta. (a) Close up images from the analyzed natural surfaces and abraded patches. Color is gaussian stretched. Analyzed points are marked in green. (b) Assignment of the bands of Reids Gap to anhydrite type II, and comparison to the hydrated phases of calcium sulfate (lab spectra). (c) Spectra acquired on veins showing clear detections of anhydrite (yellow) including a potential Nd3+ luminescent doublet in Reids Gap (blue). (d) Spectra acquired on abraded patches show clear signs of sulfates, assigned to the main peak of anhydrite for most and potential bassanite for Dragons Egg. Water band region (2,750–4,000 cm−1) lacks signs of hydration in all spectra.

samples in this area, including Uganik Island (sol 619, 1 × 10 raster with four Raman points, 400 shots) at Yori Pass outcrop, where anhydrite was detected on the white spots of the abraded patch (Clavé, Beyssac, et al., 2023).

Further detections of calcium sulfate, primarily anhydrite, were observed by Raman in the white spots of various abraded patches in the upper fan, including: Solva (sol 751, 1 × 10 raster with four Raman points, 400 shots) at the curvilinear unit, which presents a diverse mineralogy (anhydrite, carbonate, olivine); Dragons Egg Rock (sol 862,

21699100, 2025, 11, Downloaded from https://agupubs.onlinelibrary.wiley.com/doi/10.1029/2025JE008943, Wiley Online Library on [18/11/2025]. See the Terms and Conditions (https://onlinelibrary.wiley.com/terms-and-conditions) on Wiley Online Library for rules of use; OA articles are governed by the applicable Creative Commons License

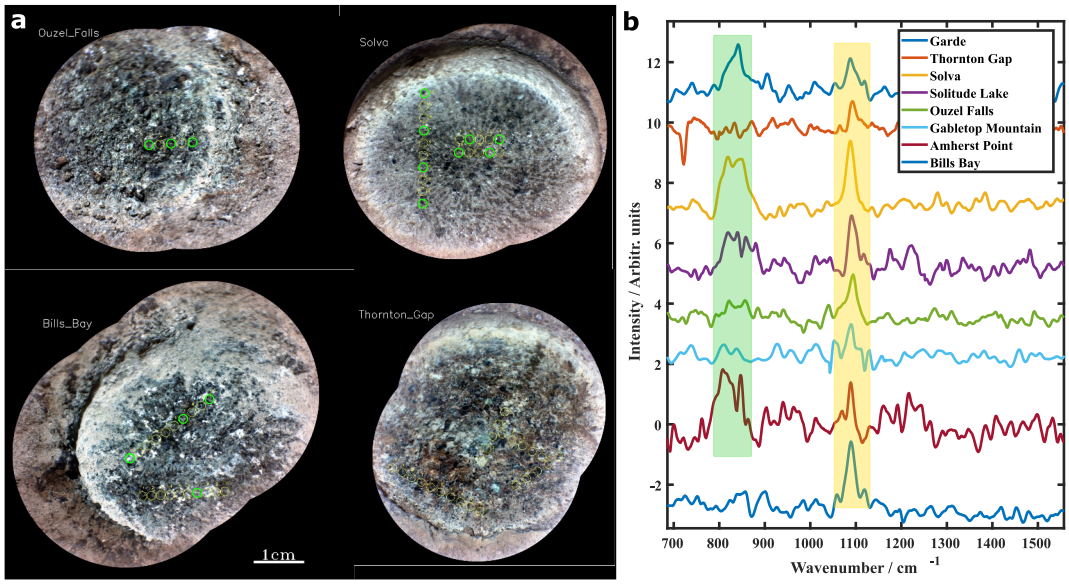

Figure 6. (a) Carbonate detections with SuperCam Raman during the first 1,000 sols of the mission on the Jezero Delta. Color is gaussian stretched. Analyzed points are marked in green (carbonate in Thornton gap is observed by averaging all points). (b) Spectra of the Fe-Mg carbonates detected for several abraded patches, showing the variability of the peak position (in cm^{-1}) for the different detections (yellow). Olivine features are observable in several of them (green).

1 × 10 raster with four Raman points, 400 shots), an abraded patch on a Pyroxene-rich boulder (Dehouck, Clavé, et al., 2024) in Mount Meeker on the Jezero upper fan, which, in addition to anhydrite, also presented a couple of points with potential bassanite (observed by a shift in the main band position, see Figure 5); and Thunderbolt peak (sol 896, 1 × 10 raster with 100 shots each) in the Willow Park outcrop at Lobe/Trough m unit, showing anhydrite.

4.2.3.4. Margin Unit

During the few sols of the margin unit campaign until sol 1,000, only one occurrence of sulfate was detected by SuperCam Raman. The Bills Bay abraded patch (sol 940, 1 × 10 raster with 4 Raman points, 400 shots) at the Turquoise Bay outcrop in the Margin unit, showed a weak elevated calcium sulfate signature –also associated with a light-toned patch in the rock and compatible with the LIBS analysis on the sample.

4.2.4. Carbonates

Carbonates are a group of minerals that contain the carbonate ion (CO^{2-}), the most intense Raman peak of which corresponds to the symmetric stretching vibration of the carbonate ion, typically found between ~1,080 cm^{-1} and ~1,100 cm^{-1}. Additional peaks can appear in the Raman spectrum, such as those around 720 cm^{-1}, associated with bending modes of the CO^{2-} ion. The position and intensity of these peaks can vary depending on the metal cation (such as Ca^{2+}, Mg^{2+}, Na^{+}, or Fe^{2+}) present in the carbonate, which helps in identifying and characterizing different carbonate minerals in a sample.

4.2.4.1. Crater Floor

Garde (sol 209, 3 × 3 raster with 9 Raman points, 100 shots per point) is one of the three abraded patches analyzed in the Séítah unit, with a single point (number 9) showing the first and only detection of carbonate in the igneous rocks of the crater floor with SuperCam Raman (Clavé, Benzerara, et al., 2023), see Figure 6. The signature is relatively weak but was confirmed thanks to consistent indications of carbonates in the LIBS and VISIR data.

4.2.4.2. Delta

In the sedimentary rocks of the Fan, carbonates were not detected with SuperCam Raman in the units of the Fan Front, but only on the upper Fan (Clavé, Beck, Dehouck, et al., 2024b; Dehouck, Forni, et al., 2024), see Figure 6), member of the Rockytop formation. In this unit, the abraded patch, named Thornton Gap (sol 486, 1 × 10 raster,

21699100, 2025, 11, Downloaded from https://agupubs.onlinelibrary.wiley.com/doi/10.1029/2025JE008943, Wiley Online Library on [18/11/2025]. See the Terms and Conditions (https://onlinelibrary.wiley.com/terms-and-conditions) on Wiley Online Library for rules of use; OA articles are governed by the applicable Creative Commons License

100 shots per point; and sols 492, 493 and 498, 1 × 5 rasters with three Raman points, 400 shots per point), shows carbonate signatures with SuperCam Raman when all the spectra acquired on this rock are averaged together. Carbonates were also identified with SuperCam LIBS (Clavé, Beck, Dehouck, et al., 2024b; Dehouck, Forni, et al., 2024), PIXL (e.g., Siebach et al., 2024) and SHERLOC (Minitti et al., 2024).

In all but one of the abraded patches subsequently analyzed on the upper Fan, we observed relatively strong carbonate signatures with SuperCam Raman: nice signatures in the curvilinear unit of the Tenby formation in Solva (sols 748 and 751, 1 × 10 rasters with 4 Raman points, 400 shots per point) and Solitude_Lake (sol 783, 1 × 10 raster with 4 Raman points, 400 shots per point); in the Blocky unit in Ouzel falls (sol 803, 1 × 5 raster with 3 Raman points, 400 shots per point); and in the Lobe/Trough m unit, Gabletop Mountain (sol 881, 1 × 10 raster with 4 Raman points, 400 shots per point). Only in Thunderbolt Peak (sol 896, 1 × 10 raster with 10 Raman points, 100 shots per point) was a carbonate signature not clear with SuperCam Raman, likely due to the low number of shots per point.

4.2.4.3. Margin Unit

Finally, the first two abraded patches performed in the Margin unit–noted for a strong carbonate signature from orbit–, showed nice carbonate signatures (Figure 6), comparable to what we observed in the upper Fan: Amherst Point (sol 925, 1 × 10 raster with 4 Raman points, 400 shots per point) in the Hans Amundsen Memorial Workspace); and Bills Bay (sols 940 and 941, 1 × 10 rasters with 4 Raman points, 400 shots per point at the Turquoise Bay outcrop of the eastern margin of the delta. These were the last detections performed by SuperCam Raman within the first 1,000 sols of the Perseverance endeavor.

5. Summary and Final Discussion

5.1. Summary on Data Acquisition and Processing

The optimization of the SuperCam Raman acquisition process has been key for maximizing the scientific return from SuperCam Raman, for which several strategies and tests were designed and executed on the Martian surface. These efforts included a trade-off analysis between the number of laser shots per point and the number of sample points analyzed to ensure efficient sample analysis. It was concluded that using 400 shots per point was advantageous, even though this approach meant that only 4 out of 10 points, or 3 out of 5 points, of the typical SuperCam rasters were analyzed. The evaluation extended to optimizing the configuration of the number of shots versus coadds to maximize SNR under real conditions of Mars. It was determined that 10 shots per coadd provided the optimal balance. Additionally, parameters such as focus distance, laser energy and laser repetition rate, and even the correlation of spectral quality with ambient temperature were tested. It was discovered that nighttime observations, which occur at lower temperatures, significantly enhance Raman spectral quality. However, nighttime operation requires careful planning and consideration due to the energy and operational constraints during Martian nights.

Another key area addressed by this work is the optimization of ground data processing methodologies for the SuperCam Raman data. The data processing pipeline implemented by the SuperCam team transforms raw, uncalibrated data into clean, scientifically usable formats through a series automated processing steps including saturation check, dark subtraction, spectral stitching, calibration and Instrument Response Function correction, denoising and removal of transient and persistent spikes from the spectra in both time and spectral domains. Additional processing is required to meticulously handle and correct artifacts such as the persistent "fiber bump" seen in the 200–500 cm^{-1} region of the spectra.

Further post-processing strategies to refine the scientific interpretations of samples include the use of mean and median spectra, coadd-to-coadd analysis for validating weak features, and cross-technique correlation with other SuperCam techniques such as LIBS and VISIR. These strategies, coupled with the possibility of averaging spectra from different points or even across multiple sols, enhance the robustness of the scientific interpretations based on SuperCam Raman data and have proven to be efficient during the exploration campaigns in Jezero.

5.2. Summary of Results From the SuperCam Calibration Targets Analysis

The analysis of the SCCTs includes the first-ever Raman spectrum acquired beyond Earth, obtained from the diamond SCCT on sol 13 of the mission. Additionally, a long-term aging experiment on the Ertalyte organic

21699100, 2025, 11, Downloaded from https://agupubs.onlinelibrary.wiley.com/doi/10.1029/2025JE008943, Wiley Online Library on [18/11/2025]. See the Terms and Conditions (https://onlinelibrary.wiley.com/terms-and-conditions) on Wiley Online Library for rules of use; OA articles are governed by the applicable Creative Commons License

sample, Bernard et al. (2025) demonstrated significant changes under Martian conditions—originally white, the sample has darkened to brown, and its Raman signal has altered. This study has even been able to correlate the degradation of the organic sample with seasonal temperature fluctuations.

The Martian environment's impact was also evident in other samples; for instance, the apatite sample showed a systematic decrease in signal intensity and an increase in background noise, effects attributed to UV radiation exposure as described by (Clavé, Beyssac, et al., 2024). Similarly, analysis of the SCCT holder's white paint revealed an interesting correlation between signal intensity and ambient temperature (Bernard et al., 2025). These findings not only highlight the influence of radiation and seasonal temperature on the integrity of these samples under Martian conditions but also helped understand how local environmental temperature variations can affect SuperCam Raman data quality, providing valuable insights for operations.

5.3. Discussion of Results With SuperCam Raman After 1,000 Sols on Mars

5.3.1. Olivine

Before Perseverance, olivine had been detected extensively in Martian meteorites (e.g., Treiman, 2005; Udry et al., 2020), and at numerous locations across the Martian surface mostly through orbital missions (Hoefen et al., 2003; Koeppen & Hamilton, 2008; Mustard et al., 2005; Ody et al., 2013), with Nili Fossae being one of the regions known for its extensive olivine-rich unit. The in situ analysis by the Perseverance rover in this region, concretely on the Séítah formation in the crater floor of the Jezero crater (Farley et al., 2022; Wiens et al., 2022), has been essential in assessing the nature of the analyzed rocks, providing strong evidence for its igneous origin (Beyssac et al., 2023; Liu et al., 2022; Udry et al., 2022). The presence of olivine in Séítah has been widely demonstrated by SuperCam analytical techniques (Beyssac et al., 2023; Mandon et al., 2023; Wiens et al., 2022) including SuperCam Raman, alongside other Perseverance instruments such as PIXL (Liu et al., 2022) or SHERLOC (Corpolongo et al., 2022). The analysis of the western fan of the delta was characterized by a lack of detections in the fan front area, compared to the identification of olivines at several locations on the upper fan, including on olivine-rich boulders (Beyssac et al., 2024) topping the fan. The lack of detection on the fan front can be interpreted as a lower presence of olivine (either due an olivine-poor sediment source or, more likely, to destruction of olivine by aqueous alteration process), but it is important to note that the overall fine-grained nature of the fan front sedimentary units (Stack et al., 2024) may have been detrimental to the SuperCam Raman due its large footprint. SuperCam Raman also detected olivines on the margin unit samples analyzed until sol 1,000.

The SuperCam Raman analysis of Martian olivines shows that spectra acquired on natural, unprepared surfaces tend to exhibit lower SNR than those obtained on fresh surfaces in abraded patches. Several non-exclusive effects can account for this: (a) thin aeolian dust mantles that reduce laser–sample coupling and increase multiple scattering (Johnson et al., 2015); (b) near-surface modification by mechanical weathering, including abrasion from saltating sand, which can chip or erode rock surfaces (Thomson et al., 2008) and locally disrupt the crystalline lattice, thereby weakening Raman scattering; and (c) irradiation-related damage, which increases defect density and fluorescence background, further lowering SNR (Royer et al., 2024). Mechanical abrasion of the surface mitigates these effects by exposing fresher grains, which explains the systematically higher SNR observed on abraded patches. A critical aspect of accurately interpreting data from olivine is the determination of their Mg# (O. Beyssac et al., 2023), which is challenging to achieve from orbital VISIR measurements due to the influence of grain size and the presence of other minerals. In this context, the in situ analysis performed by SuperCam Raman has facilitated the precise calculation of the Mg# throughout different scientific campaigns by reliably identifying the characteristic olivine doublet at ~820 and ~850 cm^{-1}. It is well known (e.g., Kuebler et al., 2006) that Raman spectra of olivines can be used to determine their Mg/Fe ratio (i.e., the forsterite/fayalite ratio, or Fo#/Fa#) through calibration curves using the band position of the olivine doublet in Raman data. However, the accuracy of these calibration curves relies heavily on the SNR of the spectra, among other factors, requiring a minimum spectral quality for reliable results. From all the available models in the literature, Kuebler et al. (2006) DB2 model (applied to the band at ~850 cm^{-1}) has demonstrated the best performance for SuperCam data with sufficient SNR. As such, the calibration from Kuebler et al. (2006) is applied to Garde and Dourbes from Séítah and Lake Haiyaha from the boulder on the upper fan, as these are samples with well-resolved olivine doublets, allowing for a comparison between the olivines found on both units.

The application of the calibration curve to Garde and Dourbes data yielded Fo# values of 59 (Beyssac et al., 2023), consistent with observations using LIBS (Beyssac et al., 2023) and other instruments such as PIXL

21699100, 2025, 11, Downloaded from https://agupubs.onlinelibrary.wiley.com/doi/10.1029/2025JE008943, Wiley Online Library on [18/11/2025]. See the Terms and Conditions (https://onlinelibrary.wiley.com/terms-and-conditions) on Wiley Online Library for rules of use; OA articles are governed by the applicable Creative Commons License

(Liu et al., 2022). The Lake Haiyaha observation of the boulder exhibits a Fo# 69 (Beyssac et al., 2024). The Fo# values obtained with SuperCam Raman (Fo# 57–69) fall well within the range reported for Martian meteorites. Olivine is abundant in the SNC suite, with magnesian compositions in chassignites and lherzolitic shergottites (Fo# 65–80), zoned crystals in olivine-phyric shergottites (Fo# 70–45), and more ferroan compositions in nakhlites (Fo# 30–45) (Treiman, 2005; Udry et al., 2020).

The Fo# plays an important role in interpreting the geology of the region, as it identifies the igneous material as primitive (higher Fo#) or evolved (lower Fo#). Being the first mineral formed during lava cooling, determining the Forsterite content helps to understand the composition of its parental magma, providing relevant information to reconstruct the geological evolution of the region. In the case of the SuperCam detections, the differences observed between the different regions likely represent different evolutions within the same olivine cumulate (Beyssac et al., 2024).The outcomes derived from SuperCam Raman data on olivines throughout the mission highlight the positive impact of Raman spectroscopy on mission results by demonstrating the capability to differentiate elemental compositions of olivines in geological units of different natures on Mars.

5.3.2. Perchlorates

Perchlorates have been identified in several locations on Mars (Archer et al., 2019; Clark & Kounaves, 2016), both through orbital spectroscopy (Ojha et al., 2015) and by surface instruments, including the Phoenix lander (Hecht et al., 2009), the Curiosity rover (Glavin et al., 2013) and even the Viking experiments (Navarro-González et al., 2010), exhibiting concentrations significantly higher than those observed for naturally occurring perchlorate-bearing terrains on Earth (Archer et al., 2019). Trace abundances of perchlorates (~0.6 ppm) have also been identified in the shergottite meteorite EETA79001 (Kounaves et al., 2014), although these concentrations are orders of magnitude lower than the wt% levels later observed in Mars soils by Phoenix (Hecht et al., 2009) and the macroscopic white patches observed in Jezero crater that were analyzed with SuperCam. Indeed, early during the crater floor campaign of the Mars 2020 mission, the SuperCam instrument achieved the in situ detection of sodium perchlorate in light-toned spots in abraded patches within the Máaz unit (Meslin et al., 2022; Wiens et al., 2022). Perchlorates have not been detected so far beyond the Jezero Crater floor. These perchlorate detections, consistent with those performed by the SHERLOC instrument (Corpolongo et al., 2022), were the first achieved by SuperCam Raman on a Martian sample, also marking the first perchlorate identification by a surface-based Raman instrument beyond Earth. The presence of perchlorates is significant for the implications it carries about the geological history of Jezero crater. Indeed, perchlorates form through aqueous alteration processes, indicating past water activity on the crater floor and suggesting episodes of both alteration and evaporation in Jezero crater. Detailed analysis of the perchlorate detections achieved by SuperCam will be addressed through dedicated manuscripts and thus is not in the scope of this work.

This detection highlights the potential of Raman spectroscopy for the straightforward identification of salts, compared to the more challenging interpretations needed from LIBS or VISIR spectra.

5.3.3. Sulfates

Sulfates on Mars have been a subject of significant scientific interest, because their formation often involves interactions with liquid water, therefore indicating past aqueous processes. The presence of sulfates has been detected and studied through various orbital, for example, (King & McLennan, 2010) and surface missions such as Opportunity in Endeavour crater (Squyres et al., 2012) or Curiosity in Gale crater (Grotzinger et al., 2012). Sulfate detections have also been confirmed by the Perseverance rover (Benison et al., 2024; Broz et al., 2024; Sun et al., 2023) and SuperCam (Dehouck, Forni, et al., 2024; Mandon et al., 2023; Nachon, Lopez-Reyes, et al., 2024, Nachon, Sieback, et al., 2024; Wiens et al., 2022; this work), on the Jezero crater, western fan and margin unit. In addition, sulfates have also been reported in Martian meteorites, particularly within the nakhlite group, where secondary assemblages of Ca-sulfates (anhydrite and gypsum) occur in veins and mesostasis regions (Treiman, 2005). These phases are widely interpreted as the product of pre-terrestrial aqueous alteration on Mars.

From an astrobiological perspective, the hydration state of sulfates is a key in order to understand their implication for habitability, since the presence of hydrated sulfates could suggest that liquid water existed long enough to allow these minerals to form (Nachon et al., 2014). Furthermore, minerals such as gypsum can provide a habitable environment as well as conditions conducive to microbial preservation (Nachon et al., 2014). Indeed, the analysis

21699100, 2025, 11, Downloaded from https://agupubs.onlinelibrary.wiley.com/doi/10.1029/2025JE008943, Wiley Online Library on [18/11/2025]. See the Terms and Conditions (https://onlinelibrary.wiley.com/terms-and-conditions) on Wiley Online Library for rules of use; OA articles are governed by the applicable Creative Commons License

of sulfates by the ChemCam instrument using LIBS with ChemCam (e.g., Nachon et al., 2014; Rapin et al., 2016, 2019) in combination with the x-ray diffractometer CheMin (Vaniman et al., 2018) provided insights as to the presence of sulfates on Gale crater, where the quantification of the hydration state of the analyzed samples was challenging. In this regard, Raman spectroscopy is highly effective in distinguishing the hydration state, as well as the cation, of sulfates. It can detect the presence or absence of hydration bands in the spectrum, but more importantly different hydration states and cations modify the position of the main bands of the spectrum. This capability makes Raman spectroscopy a valuable tool for analyzing and interpreting the hydration state of sulfates. Indeed, one of the main advantages provided by Raman spectroscopy that has been demonstrated during the Mars2020 mission so far, is that it can help discriminate between polymorphs and/or structural hydration, as for example, with Ca sulfate were it is possible to distinguish gypsum -$CaSO_4{\cdot}2H_2O$-, bassanite -$CaSO_4{\cdot}0.5H_2O$- and the three anhydrite polymorphs -$CaSO_4$ types I, II and III- (as shown in Figure 5).

In summary, the analyses performed by SuperCam Raman mostly on light-toned veins and abraded patches on the Jezero crater floor, western fan and margin unit, provided numerous sulfate detections in agreement with LIBS and VISIR spectra (Lopez-Reyes et al., 2023). The weak but discernible detections within the crater support the sulfate detections provided by the broader interpretation by all SuperCam techniques. Within the fan and margin units, the detected sulfates predominantly consisted of anhydrite (anhydrous calcium sulfate), narrowed down to Anhydrite Type II on high-quality spectra such as those on Reids Gap or Kupreanof Strait. In general, most sulfate detections by SuperCam were concentrated on the Jezero delta, their anhydrous nature notably differing from the primarily hydrated phases of Ca sulfate (bassanite) detected in other regions of Mars.

The presence of sulfates in veins, such as Reids Gap, indicates precipitation from groundwater that flowed through the rocks after their formation. Of greater interest is the fact that the bedrock, especially in certain members of the delta formation, contains a significant fraction of sulfates. This likely indicates that the lake water was being intensively evaporated and hence concentrated in salts, including Ca-sulfates (Dehouck, Forni, et al., 2024). Certain sulfate-related detections also displayed potential luminescence effects that will be part of subsequent studies. All these sulfate findings, sometimes coexisting with carbonates and/or olivine, in combination with other detections by previous missions at Endeavour and Gale craters, underscore a diverse mineralogy confirming extended aqueous processes on Mars.

5.3.4. Carbonates

Carbonates have been detected on Mars both from orbit, meteorites, and in situ by several missions. From orbit, the highest surface density of carbonates is found in the Nili Fossae region, where Jezero crater lies (e.g., Carter et al., 2023; Ehlmann, Mustard, Murchie, et al., 2008). Carbonates were also detected in outcrops exposed by impact craters (Wray et al., 2016) and in weathering profiles (Bultel et al., 2019) in the oldest terrains exposed all around the red planet. These carbonates are mostly Fe- Mg carbonates and often associated with phyllosilicates. Carbonates have also been identified in Martian meteorites, most prominently in the orthopyroxenite ALH 84001, where Mg–Fe–Ca carbonates occur as globules interpreted to record ancient low-temperature aqueous alteration on Mars (Halevy et al., 2011). Additional occurrences of secondary carbonates have been reported in the nakhlite group (Treiman, 2005). Several in situ missions also detected carbonates on the surface of Mars: at Gusev Crater (Morris et al., 2010), locally in Gale crater (Thorpe et al., 2022) and more often in Jezero Crater (Clavé, Benzerara, et al., 2023; Clavé, Beck, Dehouck, et al., 2024; Tice et al., 2022). Carbonates in Jezero were detected in larger amounts and a wider diversity than anywhere else on Mars. They were detected in both igneous rocks in the crater floor, where they are thought to derive from local alteration with low water-to-rock ratios (Clavé, Benzerara, et al., 2023; Tice et al., 2022) and in the sedimentary rocks of Jezero Western Fan (Clavé, Beck, Dehouck, et al., 2024; this work).

All these carbonate detections correspond to Fe-, Mg-rich (typically 20–30 wt.% FeO and or MgO) and relatively Ca-poor ($\leq$3–5 wt.% CaO) points based on the LIBS data, indicating that these are Fe-Mg carbonates. In this case, it is possible to use the position of the main carbonate peak in Raman to characterize the composition of the carbonates (e.g., Beck et al., 2024; Boulard et al., 2012). It is an ongoing effort within the team (preliminary results in (Clavé, Beck, Beyssacc et al., 2024; Clavé, Beck, Dehouck, et al., 2024). This is of interest for SuperCam as LIBS only sampled carbonates mixed with other mineral phases, and it is hence difficult to characterize the composition of the carbonates themselves.

21699100, 2025, 11, Downloaded from https://agupubs.onlinelibrary.wiley.com/doi/10.1029/2025JE008943, Wiley Online Library on [18/11/2025]. See the Terms and Conditions (https://onlinelibrary.wiley.com/terms-and-conditions) on Wiley Online Library for rules of use; OA articles are governed by the applicable Creative Commons License

Abundant carbonates were anticipated in Jezero crater based on orbital observations, and several formation mechanisms had been proposed, including precipitation in a lacustrine shoreline environment, carbonation of ultramafic rocks, or a detrital origin (e.g., Goudge et al., 2015; Horgan et al., 2020; Tarnas et al., 2021). In situ analyses by Perseverance, particularly SuperCam Raman, indicate that the Fe-Mg carbonates associated with olivine and silica most likely formed through in situ carbonation of ultramafic rocks (Clavé, Beck, Beyssacc et al., 2024).

6. Conclusions

The SuperCam time-resolved remote Raman instrument on the Perseverance rover has successfully demonstrated its ability to collect and process valuable scientific data on Mars, despite the inherent challenges of remote planetary exploration. This work has described the set of strategies designed and developed for optimizing the data acquisition and processing methodologies of SuperCam Raman data. Overall, these represent a sophisticated balance between automated processes and careful scientific treatment, ensuring that the data returned from Mars are both unbiased and informative.

During the first 1,000 sols on Mars, the Perseverance rover executed the crater floor and delta campaigns, at that time advancing into the Margin unit campaign. This work has reviewed the SuperCam Raman analysis conducted during this period, including both the SCCT samples as well as geologic samples from Mars, facilitating the detection and interpretation of olivines, sulfates, perchlorates and carbonates both on abraded patches and natural surfaces across Jezero.

The stand-off aspect of SuperCam Raman spectroscopy makes it significantly more challenging than in situ micro-Raman spectroscopy that is typically performed in the laboratory. Most of the Mars surface Raman signals were a few tens to over a hundred detector counts per observation, mostly on relatively fine-grained minerals. However, strong Raman signals can be obtained even at remote distances with the proper samples. This was illustrated by the Reids Gap spectra of anhydrite on sol 462 with peaks of more than 1,500 counts, or later on, when peaks with several thousand counts were obtained on a quartz target (Beck et al., 2025) acquired after Sol 1,000, while this manuscript was in preparation. We may expect to find these stronger signals from time to time in the future.

Raman spectroscopy has been essential for deciphering the geological history of the Jezero crater, providing rapid and unambiguous identification of mineral phases. It has proven especially valuable in differentiating chemistry and hydration states of sulfates and salts, and in quantifying cation content in olivine or carbonate samples. These results underscore the potential and key role that Raman spectroscopy will hold in current and future planetary exploration missions.

Appendix A: The SuperCam Team

Wiens, R.C.[1]; Cousin, A.[2]; Clegg, S.M.[3]; Gasnault, O.[2]; Maurice, S.[2]; Acosta-Maeda, T.[4]; Alberquilla, F.[5]; Alvarez-Llamas, C.[6]; Anderson, R.B.[7]; Angel, S.M.[8]; Applin, D.M.[9]; Aramendia, J.[5]; Arana, G.[5]; Bassas-Portus, M.[10]; Beal, R.[3]; Beck, P.[11]; Bedford, C.[1]; Benzerara, K.[12]; Bernard, S.[12]; Bernardi, P.[13]; Bertrand, T.[13]; Beyssac, O.[12]; Biancalani, S.[14]; Bloch, T.[15]; Bousquet, B.[16]; Bouyssou Mann, M.[15]; Brand, M.[3]; Brown, A.[17]; Brown, W.[18]; Cadu, A.[10]; Caïs, P.[19]; Caravaca, G.[20]; Castro Ortiz de Pinedo, K.[5]; Charpentier, A.[15]; Chide, B.[2]; Christensen, S.A.[21]; Clavé, E.[22]; Cloutis, E.A.[9]; Coloma, L.[5]; Comellas, J.[4]; Connell, S. A.[1]; Cornus, S.[15]; Dehouck, E.[23]; Delapp, D.[3]; Deron, R.[24]; Donny, C.[15]; Dorresoundiram, A.[13]; Dromart, G.[23]; Dubois, B.[25]; Dybdal-Nielsen, S-S.[21]; Essunfeld, A.[3]; Fabre, C.[26]; Fau, A.[2]; Fischer, W.[27]; Fornaro, T.[14]; Forni, O.[2]; Fouchet, T.[13]; Francis, R.[28]; Frydenvang, J.[21]; Gabriel, T.[7]; Gallegos, Z.[29]; García-Gómez, L.[6]; Gasda, P.[3]; Gibbons, E.[30]; Gonzalez, S.J.[31]; Gontijo, I.[28]; Grotzinger, J.[27]; Huidobro, J.[5]; Jacob, X.[32]; Jean-Rigaud, L.[15]; Johnson, J.R.[33]; Julien, J.[34]; Kalucha, H.[27]; Kelly, E.[4]; Knutsen, E.W.[35]; Lacombe, G.[15]; Lamarque, F.[15]; Lanza, N.L.[3]; Larmat, C.[3]; Laserna, J.[6]; Lasue, J.[2]; Le Deit, L.[36]; Le Mouélic, S.[36]; Legett IV, C.[3]; Leveille, R.[30]; Lewin, E.[11]; Little, C.[37]; Loche, M.[2]; Lopez-Reyes, G.[31]; Lorenz, R.D.[33]; Lorigny, E.[15]; Madariaga, J.M.[5]; Madsen, M. B.[38]; Mandon, L.[11]; Manelski, H.[1]; Mangold, N.[36]; Manrique Martínez, J.A.[31]; Oro-Marot, L.[34]; Martin, N.[1]; Martinez-Frias, J.[39]; McConnochie, T.[40]; McLennan, S.M.[41]; Melikechi, N.[42]; Meslin, P.-Y.[2]; Meunier, F.[15]; Mimoun, D.[10]; Montagnac, G.[23]; Montmessin, F.[43]; Moros, J.[6]; Moten, S.[4]; Motta, G.[44]; Mousset, V.[15]; Murdoch, N.[10];

21699100, 2025, 11, Downloaded from https://agupubs.onlinelibrary.wiley.com/doi/10.1029/2025JE008943, Wiley Online Library on [18/11/2025]. See the Terms and Conditions (https://onlinelibrary.wiley.com/terms-and-conditions) on Wiley Online Library for rules of use; OA articles are governed by the applicable Creative Commons License

Nachon, M.[45]; Nelson, T.[3]; Newell, R.T.[3]; Nicolas, C.[24]; Nikolajsen, K.[21]; O'Shea, C.[33]; Ollila, A.[3]; Orlauskis, V.[35]; Pantalacci, P.[15]; Parot, Y.[2]; Payré, V.[18]; Pilleri, P.[2]; Pilorget, C.[46]; Pinet, P.[2]; Poblacion, I.[5]; Poulet, F.[46]; Quantin-Nataf, C.[23]; Quertier, B.[19]; Rammelkamp, K.[22]; Rapin, W.[2]; Reyes-Newell, A.[3]; Reyes-Rodriguez, I.[31]; Robinson, S.[37]; Rochas, L.[15]; Root, M.[3]; Royer, C.[43]; Rull Pérez, F.[31]; Sautter, V.[12]; Sans-Jofre, P.[12]; Schröder, S.[22]; Seel, F.[22]; Sharma, S.K.[4]; Sheridan, A.[3]; Shridar, V.[28]; Sournac, A.[10]; Stcherbinine, A.[2]; Stott, A.[10]; Toplis, M.[2]; Torre-Fdez, I.[6]; Turenne, N.[9]; Tzanetos, T.[28]; Udry, A.[44]; Veneranda, M.[31]; Venhaus, D.[3]; Vogt, D.[22]; Willis, P.[28]; Wolf, U.[3]; Zastrow, A.[3]

[1] Purdue University, West Lafayette, IN, USA [2] Institut de Recherche en Astrophysique et Planétologie (IRAP), Université de Toulouse 3 Paul Sabatier, CNRS, CNES, Toulouse, France [3] Los Alamos National Laboratory (LANL), Los Alamos, NM, USA [4] University of Hawai'i at Mānoa, Honolulu, HI, USA [5] University of the Basque Country (UPV/EHU), Leioa, Bilbao, Spain [6] UMALASERLAB, Universidad de Málaga, Departamento de Química Analítica, Málaga, Spain [7] U.S. Geological Survey, Astrogeology Science Center, Flagstaff, AZ, USA [8] Department of Chemistry and Biochemistry, University of South Carolina, Columbia, SC, USA [9] University of Winnipeg, Winnipeg, MB, Canada [10] Institut Supérieur de l'Aéronautique et de l'Espace (ISAE-SUPAERO), Université de Toulouse, Toulouse, France [11] Univ. Grenoble Alpes, CNRS, IPAG, 38,000 Grenoble, France [12] IMPMC, Institut de Minéralogie, de Physique des Matériaux et de Cosmochimie, CNRS, Sorbonne Université, MNHN, Paris, France [13] LIRA, Laboratoire d'Instrumentation et de Recherche en Astrophysique, Observatoire de Paris, Université PSL, CNRS, Sorbonne Université, Université Paris Cité, Meudon, France [14] INAF, Astrophysical Observatory of Arcetri, Florence, Italy [15] Centre National d'Études Spatiales (CNES), Toulouse, France [16] Centre Lasers Intenses et Applications, CNRS, CEA, Univ. Bordeaux, France [17] Plancius Research, Severna Park, MD, USA [18] School of Earth, Environment, and Sustainability, University of Iowa, Iowa City, IA, USA [19] Laboratoire d'Astrophysique de Bordeaux, CNRS, Univ. Bordeaux, France [20] Géosciences Environnement Toulouse (GET), UMR 5563 CNRS, IRD, UT, CNES, Université de Toulouse, France [21] Globe Institute, University of Copenhagen, Copenhagen, Denmark [22] Deutsches Zentrum für Luft-und Raumfahrt (DLR), Institute of Space Research, Berlin, Germany [23] Université Claude Bernard Lyon 1, ENS de Lyon, CNRS, UJM, LGL-TPE, UMR 5276, F-69622, Villeurbanne cedex, France [24] Atos, France [25] GIS, Observatoire Midi-Pyrénées, Toulouse, France [26] GéoRessources, CNRS, Université de Lorraine, Nancy, France [27] California Institute of Technology (Caltech), Pasadena, CA, USA [28] Jet Propulsion Laboratory (JPL), California Institute of Technology, Pasadena, CA, USA [29] University of New Mexico (UNM), Albuquerque, NM, USA [30] McGill University, Montreal, QC, Canada [31] ERICA Research Group, Universidad de Valladolid, Valladolid, Spain [32] Institut de Mécanique des Fluides (IMFT), Univ. Toulouse 3 Paul Sabatier, INP, CNRS, Toulouse, France [33] Johns Hopkins University Applied Physics Laboratory (JHU/APL), Laurel, MD, USA [34] Telespazio, France [35] University of Oslo, Oslo, Norway [36] Laboratoire de Planétologie et Géosciences, CNRS UMR 6112, Nantes Université, Univ Angers, Le Mans Université, 45000 Nantes, France [37] Planetary Science Institute (PSI), Tucson, AZ, USA [38] Niels Böhr Institute, University of Copenhagen, Copenhagen, Denmark [39] Agencia Estatal Consejo Superior de Investigaciones Científicas (CSIC), Madrid, Spain [40] University of Maryland, College Park, MD, USA [41] State University of New York, Stony Brook, NY, USA [42] Department of Physics and Applied Physics, University of Massachusetts, Lowell, MA, USA [43] LATMOS, Laboratoire Atmosphères, Milieux, Observations Spatiales, CNRS, Univ. Saint-Quentin-en-Yvelines, Sorbonne Univ., France [44] University of Nevada, Las Vegas, NV, USA [45] Texas A&M University, College Station, TX, USA [46] Institut d'Astrophysique Spatiale (IAS), CNRS, Université Paris-Saclay, Orsay, France.

Conflict of Interest

The authors declare no conflicts of interest relevant to this study.

Data Availability Statement

Data acquired by the SuperCam instrument on the Perseverance rover was used. All data are publicly available at Planetary Data System (PDS) 6 months after the acquisition. The SuperCam data used in this manuscript is available at the SuperCam PDS bundle that can be located in Maurice and Wiens (2021). The software used for data processing and figure generation is Matlab R2024b (https://mathworks.com/products/matlab.html).

21699100, 2025, 11, Downloaded from https://agupubs.onlinelibrary.wiley.com/doi/10.1029/2025JE008943, Wiley Online Library on [18/11/2025]. See the Terms and Conditions (https://onlinelibrary.wiley.com/terms-and-conditions) on Wiley Online Library for rules of use; OA articles are governed by the applicable Creative Commons License

Acknowledgments
This publication is supported through Grants "PID2022-142490OB-C32" and "PCI2023-146000-2", funded by MICIU/AEI/10.13039/501100011033 and co-funded by FEDER, European Union. It is also supported by Consejeria de Educación (JCyL), Grants VA026G24 and CLU-2023-1-05. Additional support came from the European Union-NextGenerationEU that funded Programa Investigo. Furthermore, the authors thank the European Social Fund and the Consejería de Educación de Castilla y León. The authors gratefully acknowledge the support of the SIGUE-Mars Consortium (MICINN, Grant RED2022-134726-T). JA, KC, LC, IP and JMM acknowledge the support of the PAMMAT project funded the Spanish Agency for Research (Ministry of Science/European Regional Fund, Grant PID2022-142750OB-I00). Collaboration in the US was supported by the NASA Mars Exploration Program funding to the Perseverance rover team. RCW acknowledges NASA Grant NNH13ZDA018O. E.A.C. thanks the Canadian Space Agency (22EXPCOI4), and the Natural Sciences and Engineering Research Council of Canada (RGPIN-2023-03413, RTI-2018-00032).

References

Anderson, R. B., Forni, O., Cousin, A., Wiens, R. C., Clegg, S. M., Frydenvang, J., et al. (2021). Post-landing major element quantification using SuperCam laser induced breakdown spectroscopy. *Spectrochimica Acta Part B: Atomic Spectroscopy*, *188*, 106347. https://doi.org/10.1016/J.SAB.2021.106347

Angel, S. M., Gomer, N. R., Sharma, S. K., & McKay, C. (2012). Remote raman spectroscopy for planetary exploration: A review. *Applied Spectroscopy*, *66*(2), 137–150. https://doi.org/10.1366/11-06535

Archer, P. D., Ming, D. W., Sutter, B., Hogancamp, J. V., Morris, R. V., Clark, B. C., Mahaffy, P. H., Navarro-González, R., McKay, C. P., Gough, R. V., Fairen, A. G., Archer, P. D., Ming, D. W., Sutter, B., Hogancamp, J. V., Morris, R. V., Clark, B. C., et al. (2019). *Perchlorate on Mars — Overview and implications*. LPI Contribution. Retrieved from https://ui.adsabs.harvard.edu/abs/2019LPICo2089.6233A/abstract.6233.

Beck, P., Beyssac, O., Dehouck, E., Bernard, S., Pineau, M., Mandon, L., et al. (2025). From hydrated silica to quartz: Potential hydrothermal precipitates found in Jezero crater, Mars. *Earth and Planetary Science Letters*, *656*, 119256. https://doi.org/10.1016/j.epsl.2025.119256

Beck, P., Beyssac, O., Schmitt, B., Royer, C., Mandon, L., Boulard, E., et al. (2024). Quantification of crystal chemistry of Fe-Mg carbonates by raman microspectroscopy and near-infrared remote sensing. *Earth and Space Science*, *11*(9), e2024EA003666. https://doi.org/10.1029/2024EA003666

Benison, K. C., Gill, K. K., Sharma, S., Siljeström, S., Zawaski, M., Bosak, T., et al. (2024). Depositional and diagenetic sulfates of hogwallow flats and yori pass, jezero crater: Evaluating preservation potential of environmental indicators and possible biosignatures from past martian surface waters and groundwaters. *Journal of Geophysical Research: Planets*, *129*(2), e2023JE008155. https://doi.org/10.1029/2023JE008155

Bernard, S., Beyssac, O., Manrique, J. A., Lopez Reyes, G., Ollila, A., Le Mouélic, S., et al. (2025). Ageing of organic materials at the surface of Mars: A Raman study aboard perseverance. *Geochemical Perspectives Letters*, *34*, 25–30. https://doi.org/10.7185/geochemlet.2509

Bernard, S., & Papineau, D. (2014). Graphitic carbons and biosignatures. *Elements*, *10*(6), 435–440. https://doi.org/10.2113/gselements.10.6.435

Beyssac, O. (2020). New trends in Raman spectroscopy: From high-resolution geochemistry to planetary exploration. *Elements*, *16*(2), 117–122. https://doi.org/10.2138/gselements.16.2.117

Beyssac, O., Clavé, E., Udry, A., Dehouck, E., Forni, O., Quantin-Nataf, C., Lopez-Reyes, G., Beck, P., Royer, C., Gabriel, T., Kah, L. C., Schroeder, S., Johnson, J. R., Fouchet, T., Simon, J., Cousin, A., Maurice, S., Wiens, R. C., Beyssac, O., et al. (2024). What are the olivine-rich boulders in the upper fan and Margin unit at jezero crater, Mars? *LPI Contribution*, *3040*, 1493. https://ui.adsabs.harvard.edu/abs/2024LPICo3040.1493B/abstract

Beyssac, O., Forni, O., Cousin, A., Udry, A., Kah, L. C., Mandon, L., et al. (2023). Petrological traverse of the olivine cumulate Séítah formation at Jezero crater, Mars: A perspective from SuperCam onboard perseverance. *Journal of Geophysical Research: Planets*, *128*(7), e2022JE007638. https://doi.org/10.1029/2022je007638

Beyssac, O., Ollila, A. M., Arana, G., Angel, S. M., Benzerara, K., Bernard, S., et al. (2021). SuperCam's time-resolved raman and Luminescence spectroscopy onboard the perseverance Rover. *LPI Contribution*, *2548*, 1499. Retrieved from https://ui.adsabs.harvard.edu/abs/2021LPI…52.1499B/abstract

Bosak, T., Shuster, D. L., Scheller, E. L., Siljeström, S., Zawaski, M. J., Mandon, L., et al. (2024). Astrobiological potential of rocks acquired by the perseverance rover at a sedimentary fan front in jezero crater, Mars. *AGU Advances*, *5*(4), e2024AV001241. https://doi.org/10.1029/2024av001241

Böttger, U., De Vera, J. P., Fritz, J., Weber, I., Hübers, H. W., & Schulze-Makuch, D. (2012). Optimizing the detection of carotene in Cyanobacteria in a Martian regolith analogue with a Raman spectrometer for the ExoMars mission. *Planetary and Space Science*, *60*(1), 356–362. https://doi.org/10.1016/j.pss.2011.10.017

Boulard, E., Guyot, F., & Fiquet, G. (2012). The influence on Fe content on Raman spectra and unit cell parameters of magnesite-siderite solid solutions. *Physics and Chemistry of Minerals*, *39*(3), 239–246. https://doi.org/10.1007/s00269-011-0479-3

Broz, A. P., Horgan, B., Kalucha, H., Johnson, J. R., Royer, C., Dehouck, E., et al. (2024). Diagenetic history and biosignature preservation potential of fine-grained rocks at hogwallow flats, jezero crater, Mars. *Journal of Geophysical Research: Planets*, *129*(11), e2024JE008520. https://doi.org/10.1029/2024JE008520

Bultel, B., Viennet, J. C., Poulet, F., Carter, J., & Werner, S. C. (2019). Detection of carbonates in Martian weathering profiles. *Journal of Geophysical Research: Planets*, *124*(4), 989–1007. https://doi.org/10.1029/2018JE005845

Carter, J., Riu, L., Poulet, F., Bibring, J. P., Langevin, Y., & Gondet, B. (2023). A Mars orbital catalog of aqueous alteration signatures (MOCAAS). *Icarus*, *389*, 115164. https://doi.org/10.1016/j.icarus.2022.115164

Chligui, M., Guimbretiere, G., Canizares, A., Matzen, G., & Vaills, Y. (2010). New features in the Raman spectrum of Silica: Key-points in the improvement on structure knowledge. Retrieved from https://hal.science/hal-00520823

Chopelas, A. (1991). Single crystal Raman spectra of forsterite, fayalite, and monticellite. *American Mineralogist*, *76*(7–8), 1101–1109.

Clark, B. C., & Kounaves, S. P. (2016). Evidence for the distribution of perchlorates on Mars. *International Journal of Astrobiology*, *15*(4), 311–318. https://doi.org/10.1017/S1473550415000385

Clavé, E., Beck, P., Beyssac, O., Forni, O., Schröder, S., Mangold, N., et al. (2024). Carbonation of mafic rocks in the Margin unit, jezero crater, Mars. *LPI Contribution*, *3007*, 3161. https://ui.adsabs.harvard.edu/abs/2024LPICo3007.3161C/abstract

Clavé, E., Beck, P., Dehouck, E., Forni, O., Schröder, S., Mangold, N., et al. (2024). Diversity of carbonates in jezero crater, Mars, as seen with the SuperCam instrument. *LPI Contribution*, *3040*, 1829. https://ui.adsabs.harvard.edu/abs/2024LPICo3040.1829C/abstract

Clavé, E., Benzerara, K., Meslin, P. Y., Forni, O., Royer, C., Mandon, L., et al. (2023). Carbonate detection with SuperCam in igneous rocks on the floor of jezero crater, Mars. *Journal of Geophysical Research: Planets*, *128*(6), e2022JE007463. https://doi.org/10.1029/2022je007463

Clavé, E., Beyssac, O., Bernard, S., Royer, C., Lopez-Reyes, G., Schröder, S., et al. (2024). Radiation-induced alteration of apatite on the surface of Mars: First in situ observations with SuperCam Raman onboard perseverance. *Scientific Reports 2024*, *14*(1), 1–12. https://doi.org/10.1038/s41598-024-61494-5

Clavé, E., Beyssac, O., Lopez-Reyes, G., Ollila, A., Fornaro, T., Willis, P., Bousquet, B., Schröder, S., Williford, K., Wiens, R. C., Maurice, S., Clavé, E., Beyssac, O., Lopez-Reyes, G., Ollila, A., Fornaro, T., Willis, P., et al. (2023). Interpreting the continuum signal in the raman spectra acquired with SuperCam in jezero crater, Mars. *LPI Contribution*, *2806*, 1898. https://ui.adsabs.harvard.edu/abs/2023LPICo2806.1898C/abstract

Clavé, E., Lopez-Reyes, G., Beyssac, O., Forni, O., Ollila, A., Schröder, S., et al. (2024). *Getting the Most out of the SuperCam raman dataset with unsupervised machine learning: Characterization of mineral signatures and their distribution* (Vol. 3040). LPI Contribution. Retrieved from https://ui.adsabs.harvard.edu/abs/2024LPICo3040.1828C/abstract.1828.

Corpolongo, A., Jakubek, R. S., Asher, S. A., Baker, D., Beegle, L. W., Berger, E. L., et al. (2022). SHERLOC Raman mineral detections of the Mars 2020 crater floor campaign. *Journal of Geophysical Research: Planets*, *128*(3), e2022JE007455. https://doi.org/10.1029/2022JE007455

21699100, 2025, 11, Downloaded from https://agupubs.onlinelibrary.wiley.com/doi/10.1029/2025JE008943, Wiley Online Library on [18/11/2025]. See the Terms and Conditions (https://onlinelibrary.wiley.com/terms-and-conditions) on Wiley Online Library for rules of use; OA articles are governed by the applicable Creative Commons License

Cousin, A., Sautter, V., Fabre, C., Dromart, G., Montagnac, G., Drouet, C., et al. (2022). SuperCam calibration targets on board the perseverance rover: Fabrication and quantitative characterization. *Spectrochimica Acta–Part B Atomic Spectroscopy*, *188*, 106341. https://doi.org/10.1016/j.sab.2021.106341

Dehouck, E., Clavé, E., Beyssac, O., Quantin-Nataf, C., Udry, A., Forni, O., et al. (2024). *Pristine pyroxene-bearing boulders analyzed by SuperCam in the jezero Western fan, Mars* (Vol. 3040). LPI Contribution. Retrieved from https://ui.adsabs.harvard.edu/abs/2024LPICo3040.1967D/abstract.1967.

Dehouck, E., Forni, O., Quantin-Nataf, C., Beck, P., Mangold, N., Beyssac, O., et al. (2024). Chemostratigraphy and mineralogy of the jezero Western fan as seen by the SuperCam instrument: Evidence for a complex aqueous history and variable alteration conditions. *LPI Contribution*, *3007*, 3364. https://ui.adsabs.harvard.edu/abs/2024LPICo3007.3364D/abstract

Edwards, C. S., & Ehlmann, B. (2015). Carbon sequestration on Mars. *Geology*, *43*(10), 863–866. https://doi.org/10.1130/G36983.1

Ehlmann, B. L., Mustard, J. F., Fassett, C. I., Schon, S. C., Head, J. W., Marais, D. J. D., et al. (2008). Clay minerals in delta deposits and organic preservation potential on Mars. *Nature Geoscience*, *1*(6), 355–358. https://doi.org/10.1038/ngeo207

Ehlmann, B. L., Mustard, J. F., Murchie, S. L., Poulet, F., Bishop, J. L., Brown, A. J., et al. (2008). Orbital identification of carbonate-bearing rocks on Mars. *Science*, *322*(5909), 1828–1832. https://doi.org/10.1126/science.1164759

Farley, K. A., Stack, K. M., Shuster, D. L., Horgan, B. H. N., Hurowitz, J. A., Tarnas, J. D., et al. (2022). Aqueously altered igneous rocks sampled on the floor of Jezero crater, Mars. *Science*, *377*(6614), eabo2196. https://doi.org/10.1126/science.abo2196

Farley, K. A., Williford, K. H., Stack, K. M., Bhartia, R., Chen, A., de la Torre, M., et al. (2020). Mars 2020 mission overview. *Space Science Reviews*, *216*(8), 1–41. https://doi.org/10.1007/S11214-020-00762-Y

Glavin, D. P., Freissinet, C., Miller, K. E., Eigenbrode, J. L., Brunner, A. E., Buch, A., et al. (2013). Evidence for perchlorates and the origin of chlorinated hydrocarbons detected by SAM at the Rocknest aeolian deposit in gale Crater. *Journal of Geophysical Research: Planets*, *118*(10), 1955–1973. https://doi.org/10.1002/JGRE.20144

Goudge, T. A., Aureli, K. L., Head, J. W., Fassett, C. I., & Mustard, J. F. (2015). Classification and analysis of candidate impact crater-hosted closed-basin lakes on Mars. *Icarus*, *260*, 346–367. https://doi.org/10.1016/j.icarus.2015.07.026

Grotzinger, J. P., Crisp, J., Vasavada, A. R., Anderson, R. C., Baker, C. J., Barry, R., et al. (2012). Mars science Laboratory mission and science investigation. *Space Science Reviews*, *170*(1–4), 5–56. https://doi.org/10.1007/S11214-012-9892-2

Halevy, I., Fischer, W. W., & Eiler, J. M. (2011). Carbonates in the Martian meteorite Allan Hills 84001 formed at 18 ± 4°C in a near-surface aqueous environment. *Proceedings of the National Academy of Sciences of the United States of America*, *108*(41), 16895–16899. https://doi.org/10.1073/pnas.1109444108

Hecht, M. H., Kounaves, S. P., Quinn, R. C., West, S. J., Young, S. M. M., Ming, D. W., et al. (2009). Detection of perchlorate and the soluble chemistry of martian soil at the Phoenix lander site. *Science*, *325*(5936), 64–67. https://doi.org/10.1126/science.1172466

Hoefen, T. M., Clark, R. N., Bandfield, J. L., Smith, M. D., Pearl, J. C., & Christensen, P. R. (2003). Discovery of olivine in the nili fossae region of Mars. *Science*, *302*(5645), 627–630. https://doi.org/10.1126/science.1089647

Horgan, B., Anderson, R. B., Dromart, G., Amador, E. S., & Rice, M. S. (2020). The mineral diversity of Jezero crater: Evidence for possible lacustrine carbonates on Mars. *Icarus*, *339*, 113526. https://doi.org/10.1016/j.icarus.2019.113526

Horgan, B., Garczynski, B., Barnes, R., Bedford, C., Cardarelli, E. L., Clavé, E., et al. (2024). Exploration of carbonate-rich rocks in the margin unit by the perseverance rover in jezero crater. *LPI Contribution*, *3007*, 3543. https://ui.adsabs.harvard.edu/abs/2024LPICo3007.3543H/abstract

Johnson, J. R., Bell, J. F., Bender, S., Blaney, D., Cloutis, E., DeFlores, L., et al. (2015). ChemCam passive reflectance spectroscopy of surface materials at the curiosity landing site, Mars. *Icarus*, *249*, 74–92. https://doi.org/10.1016/J.ICARUS.2014.02.028

Kelly, E. M., Acosta, T., Lopez-reyes, G., Egan, M. J., Angel, S. M., Ollila, A. M., Beyssac, O., Clavé, E., Sharma, S. K., Weins, R. C., Team, S., Kelly, E. M., Acosta, T., Lopez-reyes, G., Egan, M. J., Angel, S. M., Ollila, A. M., et al. (2023). Fiber- induced raman signal (FIRS) analysis from the perseverance rover of the jezero crater floor. *LPI Contribution*, *2806*, 1786. https://ui.adsabs.harvard.edu/abs/2023LPICo2806.1786K/abstract

King, P. L., & McLennan, S. M. (2010). Sulfur on Mars. *Elements*, *6*(2), 107–112. https://doi.org/10.2113/gselements.6.2.107

Koeppen, W. C., & Hamilton, V. E. (2008). Global distribution, composition, and abundance of olivine on the surface of Mars from thermal infrared data. *Journal of Geophysical Research*, *113*(E5), 5001. https://doi.org/10.1029/2007JE002984

Kounaves, S. P., Carrier, B. L., O'Neil, G. D., Stroble, S. T., & Claire, M. W. (2014). Evidence of martian perchlorate, chlorate, and nitrate in Mars meteorite EETA79001: Implications for oxidants and organics. *Icarus*, *229*, 206–213. https://doi.org/10.1016/j.icarus.2013.11.012

Kuebler, K. E., Jolliff, B. L., Wang, A., & Haskin, L. A. (2006). Extracting olivine (Fo–Fa) compositions from Raman spectral peak positions. *Geochimica et Cosmochimica Acta*, *70*(24), 6201–6222. https://doi.org/10.1016/J.GCA.2006.07.035

Lam, P. K., Yu, R., Lee, L. W., & Snanul, S. K. (1990). Structural distortions and vibrational modes in Mg_2SiO_4. *American Mineralogist*, *75*, 109–110.

Legett, C., Newell, R. T., Reyes-Newell, A. L., Nelson, A. E., Bernardi, P., Bender, S. C., et al. (2022). Optical calibration of the SuperCam instrument body unit spectrometers. *Applied Optics*, *61*(11), 2967. https://doi.org/10.1364/AO.447680

Liu, Y., Tice, M. M., Schmidt, M. E., Treiman, A. H., Kizovski, T. V., Hurowitz, J. A., et al. (2022). An olivine cumulate outcrop on the floor of Jezero crater, Mars. *Science*, *377*(6614), 1513–1519. https://doi.org/10.1126/science.abo2756

Lopez-Reyes, G., Moral, A. G., Rull, F., Rodriguez, J. A., Pilorget, C., Bibring, J. P., & Vago, J. L. (2018). RLS calibration target design to allow onboard combined science between RLS and MicrOmega instruments on the ExoMars rover. *Georaman 2018*.

Lopez-Reyes, G., Nachon, M., Veneranda, M., Beyssac, O., Madariaga, J. M., Manrique, J. A., et al. (2023). Anhydrite detections by raman spectroscopy with supercam at the jezero Delta, Mars. *LPI Contribution*, *2806*, 1721. https://ui.adsabs.harvard.edu/abs/2023LPICo2806.1721L/abstract

Madariaga, J. M., Aramendia, J., Arana, G., Castro, K., Gómez-Nubla, L., Fdez-Ortiz de Vallejuelo, S., et al. (2022). Homogeneity assessment of the SuperCam calibration targets onboard rover perseverance. *Analytica Chimica Acta*, *1209*, 339837. https://doi.org/10.1016/j.aca.2022.339837

Mandon, L., Parkes Bowen, A., Quantin-Nataf, C., Bridges, J. C., Carter, J., Pan, L., et al. (2021). Morphological and spectral diversity of the clay-bearing unit at the ExoMars landing site Oxia Planum. *Astrobiology*, *21*(4), 464–480. https://doi.org/10.1089/ast.2020.2292

Mandon, L., Quantin-Nataf, C., Royer, C., Beck, P., Fouchet, T., Johnson, J. R., et al. (2023). Reflectance of jezero crater floor: 2. Mineralogical interpretation. *Journal of Geophysical Research: Planets*, *128*(7), e2022JE007450. https://doi.org/10.1029/2022je007450

Manrique, J. A., Clave, E., Lopez-Reyes, G., Beyssac, O., Bousquet, B., Forni, O., et al. (2022). Correction of the instrument optical fiber contribution to SuperCam Raman spectra. *GeoRaman 2022*.

Manrique, J. A., Lopez-Reyes, G., Cousin, A., Rull, F., Maurice, S., Wiens, R. C., et al. (2020). SuperCam calibration targets: Design and development. *Space Science Reviews*, *216*(8), 1–28. https://doi.org/10.1007/s11214-020-00764-w

21699100, 2025, 11, Downloaded from https://agupubs.onlinelibrary.wiley.com/doi/10.1029/2025JE008943, Wiley Online Library on [18/11/2025]. See the Terms and Conditions (https://onlinelibrary.wiley.com/terms-and-conditions) on Wiley Online Library for rules of use; OA articles are governed by the applicable Creative Commons License

Manrique, J. A., Lopez-Reyes, G., Veneranda, M., Sanz-Arranz, A., Santamaria, J. S., Julve- Gonzalez, S., et al. (2024). Characterization of SimulCam, a standoff Raman system for scientific support of SuperCam operations on Mars. *Advances in Space Research*, *74*(8), 3855–3876. https://doi.org/10.1016/j.asr.2024.08.007

Martinez, G. M., Lasue, J., Meslin, P.-Y., Chide, B., Caravaca, G., Lopez-Reyes, G., et al. (2023). The first frost detection campaign by the Mars 2020 perseverance rover: Implementation and results. *LPI Contribution*, *2806*, 2184. https://ui.adsabs.harvard.edu/abs/2023LPICo2806.2184M/abstract

Maurice, S., Chide, B., Murdoch, N., Lorenz, R. D., Mimoun, D., Wiens, R. C., et al. (2022). In situ recording of Mars soundscape. *Nature 2022 605:7911*, *605*(7911), 653–658. https://doi.org/10.1038/s41586-022-04679-0

Maurice, S., & Wiens, R. C. (2021). Mars 2020 SuperCam bundle. https://doi.org/10.17189/1522646

Maurice, S., Wiens, R. C., Bernardi, P., Caïs, P., Robinson, S., Nelson, T., et al. (2021). The SuperCam instrument suite on the Mars 2020 rover: Science objectives and mast-unit description. *Space Science Reviews*, *217*(3), 1–108. https://doi.org/10.1007/s11214-021-00807-w

Maurice, S., Wiens, R. C., Saccoccio, M., Barraclough, B., Gasnault, O., Forni, O., et al. (2012). The ChemCam instrument suite on the Mars science laboratory (MSL) rover: Science objectives and mast unit description. *Space Science Reviews*, *170*(1–4), 95–166. https://doi.org/10.1007/s11214-012-9912-2

Meslin, P.-Y., Forni, O., Beck, P., Cousin, A., Beyssac, O., Lopez-Reyes, G., et al. (2022). Evidence for perchlorate and sulfate salts in jezero crater, Mars, from supercam observations. *LPI Contribution*, *2678*, 2694. https://ui.adsabs.harvard.edu/abs/2022LPICo2678.2694M/abstract

Minitti, M. E., Bhartia, R., Sharma, S., Murphy, A. E., Uckert, K., Phua, Y., et al. (2024). *Investigating minerals and organics in the jezero Delta utilizing SHERLOC texture, fluorescence, and hydration observations* (Vol. 3040). LPI Contribution. Retrieved from https://ui.adsabs.harvard.edu/abs/2024LPICo3040.1935M/abstract.1935.

Montagnac, G., Dromart, G., Beck, P., Mercier, F., Reynard, B., Cousin, A., et al. (2018). Spark plasma sintering preparation of reference targets for field spectroscopy on Mars. *Journal of Raman Spectroscopy*, *49*(9), 1419–1425. https://doi.org/10.1002/jrs.5406

Moral, A. G., Mora, J., Prieto-Ballesteros, O., Ercilla, O., Lopez-Reyes, G., Canora, C. P., et al. (2023). Deuterated PET: The new verification target of the Raman spectrometer for the MMX mission to explore phobos. *Journal of Raman Spectroscopy*, *54*(11), 1268–1279. https://doi.org/10.1002/jrs.6569

Morris, R. V., Ruff, S. W., Gellert, R., Ming, D. W., Arvidson, R. E., Clark, B. C., et al. (2010). Identification of carbonate-rich outcrops on Mars by the spirit rover. *Science*, *329*(5990), 421–424. https://doi.org/10.1126/science.1189667

Mustard, J. F., Poulet, F., Gendrin, A., Bibring, J. P., Langevin, Y., Gondet, B., et al. (2005). Olivine and pyroxene diversity in the crust of Mars. *Science*, *307*(5715), 1594–1597. https://doi.org/10.1126/science.1109098

Nachon, M., Clegg, S. M., Mangold, N., Schröder, S., Kah, L. C., Dromart, G., et al. (2014). Calcium sulfate veins characterized by ChemCam/Curiosity at Gale crater, Mars. *Journal of Geophysical Research: Planets*, *119*(9), 1991–2016. https://doi.org/10.1002/2013JE004588

Nachon, M., Lopez-Reyes, G., Meslin, P. Y., Ollila, A., Mandon, L., Clavé, E., et al. (2024). Light-Toned veins and material in jezero crater, Mars, as seen In-Situ via NASA's perseverance rover (Mars 2020 mission): Stratigraphic distribution and compositional results. *LPI Contribution*, *3040*, 2349. https://ui.adsabs.harvard.edu/abs/2024LPICo3040.2349N/abstract

Nachon, M., Lopez-Reyes, G., Meslin, P.-Y., Ollila, A., Mandon, L., Clavé, E., et al. (2023). Light-toned veins and material in jezero crater, Mars, as seen In-Situ via NASA's perseverance rover (Mars 2020 mission): Stratigraphic distribution and compositional results from the SuperCam instrument. *LPI Contribution*, *2806*, 2673. https://ui.adsabs.harvard.edu/abs/2023LPICo2806.2673N/abstract

Nachon, M., Siebach, K. L., Sholes, S., Sun, V. Z., Del Sesto, T., Weiss, B. P., et al. (2024). *Overview of the Mars 2020 mission perseverance rover third science campaign: Exploring jezero crater's upper fan* (Vol. 3040). LPI Contribution. Retrieved from https://ui.adsabs.harvard.edu/abs/2024LPICo3040.2317N/abstract.2317.

Navarro-González, R., Vargas, E., De La Rosa, J., Raga, A. C., & McKay, C. P. (2010). Reanalysis of the viking results suggests perchlorate and organics at midlatitudes on Mars. *Journal of Geophysical Research*, *115*(E12), 12010. https://doi.org/10.1029/2010JE003599

Ody, A., Poulet, F., Bibring, J. P., Loizeau, D., Carter, J., Gondet, B., & Langevin, Y. (2013). Global investigation of olivine on Mars: Insights into crust and mantle compositions. *Journal of Geophysical Research E: Planets*, *118*(2), 234–262. https://doi.org/10.1029/2012JE004149

Ojha, L., Wilhelm, M. B., Murchie, S. L., Mcewen, A. S., Wray, J. J., Hanley, J., et al. (2015). Spectral evidence for hydrated salts in recurring slope lineae on Mars. *Nature Geoscience 2015*, *8*(11), 829–832. https://doi.org/10.1038/ngeo2546

Prieto-Taboada, N., Gómez-Laserna, O., Martínez-Arkarazo, I., Olazabal, M. Á., & Madariaga, J. M. (2014). Raman spectra of the different phases in the CaSO4-H2O system. *Analytical Chemistry*, *86*(20), 10131–10137. https://doi.org/10.1021/ac501932f

Rapin, W., Ehlmann, B. L., Dromart, G., Schieber, J., Thomas, N. H., Fischer, W. W., et al. (2019). An interval of high salinity in ancient Gale crater lake on Mars. *Nature Geoscience*, *12*(11), 889–895. https://doi.org/10.1038/s41561-019-0458-8

Rapin, W., Meslin, P. Y., Maurice, S., Vaniman, D., Nachon, M., Mangold, N., et al. (2016). Hydration state of calcium sulfates in Gale crater, Mars: Identification of bassanite veins. *Earth and Planetary Science Letters*, *452*, 197–205. https://doi.org/10.1016/j.epsl.2016.07.045

Royer, C., Bernard, S., Beyssac, O., Balan, E., Forni, O., Gauthier, M., et al. (2024). Impact of UV radiation on the Raman and infrared spectral signatures of sulfates, phosphates and carbonates: Implications for Mars exploration. *Icarus*, *410*, 115894. https://doi.org/10.1016/j.icarus.2023.115894

Rull, F., Vegas, A., Sansano, A., & Sobron, P. (2011). Analysis of arctic ices by Remote Raman spectroscopy. *Spectrochimica Acta Part A: Molecular and Biomolecular Spectroscopy*, *80*(1), 148–155. https://doi.org/10.1016/j.saa.2011.04.007

Sharma, S. K., Lucey, P. G., Ghosh, M., Hubble, H. W., & Horton, K. A. (2003). Stand-off Raman spectroscopic detection of minerals on planetary surfaces. *Spectrochimica Acta Part A: Molecular and Biomolecular Spectroscopy*, *59*(10), 2391–2407. https://doi.org/10.1016/S1386-1425(03)00080-5

Sharma, S. K., Misra, A. K., Lucey, P. G., & Lentz, R. C. F. (2009). A combined remote Raman and LIBS instrument for characterizing minerals with 532 nm laser excitation. *Spectrochimica Acta Part A: Molecular and Biomolecular Spectroscopy*, *73*(3), 468–476. https://doi.org/10.1016/j.saa.2008.08.005

Sharma, S. K., Misra, A. K., Lucey, P. G., Wiens, R. C., & Clegg, S. M. (2007). Combined remote LIBS and Raman spectroscopy at 8.6m of sulfur-containing minerals, and minerals coated with hematite or covered with basaltic dust. *Spectrochimica Acta. Part A, Molecular and Biomolecular Spectroscopy*, *68*(4), 1036–1045. https://doi.org/10.1016/j.saa.2007.06.046

Sharma, S. K., Olilla, A. M., Lopez-Reyes, G., Madariaga, J. M., Angel, S. M., Manrique, J. A., et al. (2023). Performance of SuperCam's remote raman System at jezero crater, Mars. *LPI Contribution*, *2806*, 1891. https://ui.adsabs.harvard.edu/abs/2023LPICo2806.1891S/abstract

Sharma, S. K., Ollila, A. M., Madariaga, J. M., Cousin, A., Angel, S. M., Aramendia, J., et al. (2023). *Sulfate detection with SuperCam's remote raman System in the jezero crater, Mars*. AGU Fall Meeting, 2023. Retrieved from https://ui.adsabs.harvard.edu/abs/2023AGUFM.P51B..04S/abstract.P51B-04.

Siebach, K., Nachon, M., Sholes, S., Sun, V. Z., Del Sesto, T., Weiss, B. P., et al. (2023). *Overview of perseverance's upper fan campaign*. AGU Fall Meeting, 2023. Retrieved from https://ui.adsabs.harvard.edu/abs/2023AGUFM.P41E3232S/abstract.P41E-3232.

21699100, 2025, 11, Downloaded from https://agupubs.onlinelibrary.wiley.com/doi/10.1029/2025JE008943, Wiley Online Library on [18/11/2025]. See the Terms and Conditions (https://onlinelibrary.wiley.com/terms-and-conditions) on Wiley Online Library for rules of use; OA articles are governed by the applicable Creative Commons License

Siebach, K. L., Tice, M. M., Hurowitz, J. A., Moreland, E. L., Van Beek, J. K., Kizovski, T. V., Schmidt, M., O'Neil, L. P., Treiman, A. H., Allwood, A. C., Cable, M. L., Nachon, M., Gupta, S., Siebach, K. L., Tice, M. M., Hurowitz, J. A., Moreland, E. L., Van Beek, J. K., Kizovski, T. V., et al. (2024). PIXL analyses of sedimentary rocks in the Mars 2020 perseverance upper fan campaign in jezero crater. *LPI Contribution*, *3040*, 2365. https://ui.adsabs.harvard.edu/abs/2024LPICo3040.2365S/abstract

Simon, J. I., Hickman-Lewis, K., Cohen, B. A., Mayhew, L. E., Shuster, D. L., Debaille, V., et al. (2023). Samples collected from the floor of jezero crater with the Mars 2020 perseverance rover. *Journal of Geophysical Research: Planets*, *128*(6), e2022JE007474. https://doi.org/10.1029/2022JE007474

Squyres, S. W., Arvidson, R. E., Bell, J. F., Calef, F., Clark, B. C., Cohen, B. A., et al. (2012). Ancient impact and aqueous processes at endeavour crater, Mars. *Science*, *336*(6081), 570–576. https://doi.org/10.1126/science.1220476

Stack, K. M., Ives, L. R. W., Gupta, S., Lamb, M. P., Tebolt, M., Caravaca, G., et al. (2024). Sedimentology and stratigraphy of the shenandoah Formation, Western fan, jezero crater, Mars. *Journal of Geophysical Research: Planets*, *129*(2), e2023JE008187. https://doi.org/10.1029/2023JE008187

Sun, V. Z., Hand, K. P., Stack, K. M., Farley, K. A., Simon, J. I., Newman, C., et al. (2023). Overview and results from the Mars 2020 perseverance Rover's first science campaign on the jezero crater floor. *Journal of Geophysical Research: Planets*, *128*(6), e2022JE007613. https://doi.org/10.1029/2022JE007613

SuperCam Raman Mineral detections table compiled in NASA's Planetary Data System repository. (n.d.). SuperCam Raman Mineral detections table compiled in NASA's Planetary Data System repository. Retrieved January 10, 2025, from Retrieved from https://pds-geosciences.wustl.edu/m2020/urn-nasa-pds-mars2020_supercam/data_derived_spectra/

Tarnas, J. D., Stack, K. M., Parente, M., Koeppel, A. H. D., Mustard, J. F., Moore, K. R., et al. (2021). Characteristics, origins, and biosignature preservation potential of carbonate-bearing rocks within and outside of jezero crater. *Journal of Geophysical Research: Planets*, *126*(11), e2021JE006898. https://doi.org/10.1029/2021JE006898

Thomson, B. J., Bridges, N. T., & Greeley, R. (2008). Rock abrasion features in the Columbia Hills, Mars. *Journal of Geophysical Research*, *113*(8), 8010. https://doi.org/10.1029/2007JE003018

Thorpe, M. T., Bristow, T. F., Rampe, E. B., Tosca, N. J., Grotzinger, J. P., Bennett, K. A., et al. (2022). Mars science laboratory CheMin data from the Glen Torridon region and the significance of lake-groundwater interactions in interpreting mineralogy and sedimentary history. *Journal of Geophysical Research: Planets*, *127*(11), e2021JE007099. https://doi.org/10.1029/2021JE007099

Tice, M. M., Hurowitz, J. A., Allwood, A. C., Jones, M. W. M., Orenstein, B. J., Davidoff, S., et al. (2022). Alteration history of Séítah formation rocks inferred by PIXL x-ray fluorescence, x-ray diffraction, and multispectral imaging on Mars. *Science Advances*, *8*(47), 9084. https://doi.org/10.1126/sciadv.abp9084

Treiman, A. H. (2005). The nakhlite meteorites: Augite-rich igneous rocks from Mars. *Geochemistry*, *65*(3), 203–270. https://doi.org/10.1016/j.chemer.2005.01.004

Udry, A., Howarth, G. H., Herd, C. D. K., Day, J. M. D., Lapen, T. J., & Filiberto, J. (2020). What Martian meteorites reveal about the interior and surface of Mars. *Journal of Geophysical Research: Planets*, *125*(12), e2020JE006523. https://doi.org/10.1029/2020JE006523

Udry, A., Ostwald, A., Sautter, V., Cousin, A., Beyssac, O., Forni, O., et al. (2022). A Mars 2020 Perseverance SuperCam Perspective on the Igneous Nature of the Máaz formation at Jezero crater and link with Séítah, Mars. *Journal of Geophysical Research: Planets*, *7*(128), e2022JE007440. https://doi.org/10.1029/2022JE007440

Vaniman, D. T., Martínez, G. M., Rampe, E. B., Bristow, T. F., Blake, D. F., Yen, A. S., et al. (2018). Gypsum, bassanite, and anhydrite at Gale crater, Mars. *American Mineralogist*, *103*(7), 1011–1020. https://doi.org/10.2138/AM-2018-6346

Veneranda, M., Sanz-Arranz, A., Manrique, J. A., Saiz, J., Garcia-Prieto, C., Pascual-Sánchez, E., et al. (2021). Analytical database of Martian minerals (ADaMM): Project synopsis and Raman data overview. *Journal of Raman Spectroscopy*, *53*(3), 364–381. https://doi.org/10.1002/jrs.6215

Wiens, R. C., Maurice, S., Lasue, J., Forni, O., Anderson, R. B., Clegg, S., et al. (2013). Pre-flight calibration and initial data processing for the ChemCam laser-induced breakdown spectroscopy instrument on the Mars Science Laboratory rover. *Spectrochimica Acta Part B: Atomic Spectroscopy*, *82*, 1–27. https://doi.org/10.1016/j.sab.2013.02.003

Wiens, R. C., Maurice, S., Robinson, S. H., Nelson, A. E., Cais, P., Bernardi, P., et al. (2021). The SuperCam instrument suite on the NASA Mars 2020 rover: Body unit and combined System tests. *Space Science Reviews*, *217*(1), 1–87. https://doi.org/10.1007/S11214-020-00777-5

Wiens, R. C., Maurice, S., & Rull Perez, F. (2017). The SuperCam remote sensing instrument suite for the Mars 2020 rover mission: A preview. *Spectroscopy*, *32*(5).

Wiens, R. C., Sharma, S. K., Thompson, J., Misra, A., & Lucey, P. G. (2005). Joint analyses by laser-induced breakdown spectroscopy (LIBS) and Raman spectroscopy at stand-of distances. *Spectrochimica Acta. Part A, Molecular and Biomolecular Spectroscopy*, *61*(10), 2324–2334. https://doi.org/10.1016/J.SAA.2005.02.031

Wiens, R. C., Udry, A., Beyssac, O., Quantin-Nataf, C., Mangold, N., Cousin, A., et al. (2022). Compositionally and density stratified igneous terrain in Jezero crater, Mars. *Science Advances*, *8*(34), 3399. https://doi.org/10.1126/sciadv.abo3399

Wray, J. J., Murchie, S. L., Bishop, J. L., Ehlmann, B. L., Milliken, R. E., Wilhelm, M. B., et al. (2016). Orbital evidence for more widespread carbonate-bearing rocks on Mars. *Journal of Geophysical Research: Planets*, *121*(4), 652–677. https://doi.org/10.1002/2015JE004972

Zastrow, A. M., & Glotch, T. D. (2021). Distinct carbonate lithologies in jezero crater, Mars. *Geophysical Research Letters*, *48*(9), e2020GL09236. https://doi.org/10.1029/2020GL092365

21699100, 2025, 11, Downloaded from https://agupubs.onlinelibrary.wiley.com/doi/10.1029/2025JE008943, Wiley Online Library on [18/11/2025]. See the Terms and Conditions (https://onlinelibrary.wiley.com/terms-and-conditions) on Wiley Online Library for rules of use; OA articles are governed by the applicable Creative Commons License